Chemical Sensing Using Polypyrrole Actuators

Ciarán Smyth B.Sc.

Thesis submitted for the Degree of Master of Science

Supervisor: Professor Dermot Diamond

Dublin City University June 2007

Declaration

I hereby certify that this material, which I now submit for assessment on the programme of study leading to the award of Masters of Science is entirely my own work and has not been taken from the work of others save and to the extent that such work has been cited and acknowledged within the text of my work.

Signed: Ciarán Smyth

Ciarán Smyth

ID No.: 50324876

Date: 19/09/07

Abstract

In the modern age methods for the calibration of sensors have become particularly important. Situations can arise where the deployment of sensors in the field, particularly in bulk, could be augmented to a very useful degree through the application of some form of autonomous monitoring system. This system would ideally be capable of taking a measurement, relaying the data to a central database and then re-setting the sensor to a default form. Inherently conducting polymers (ICPs) are useful in modern research due to their highly conductive properties when doped, and their concurrent mechanical flexibility. The ICP polypyrrole can be prepared as an electromechanical actuator, capable of operation under low applied power.

Through the application of colorimetric dyes to the polypyrrole actuators simple sensors can be developed with the actuator acting as a delivery mechanism of the sensor to the sample of interest. This concept has been developed through the use of LED-based detectors and RGB-analysis of digital images.

Table of Contents

1. Introduction

1.1 Principles of Chemical Sensing

A selective response to a given analyte is the basis upon which sensor research is based. Examples of such responses involve enzyme-substrate reactions and antibody-antigen reactions. Of course inducing these reactions to occur is entirely fruitless if there are no competent ways of harvesting the information through some kind of transduction mechanism. This is generally done via the transmission of electrical or optical signals, and the two techniques most commonly employed to generate such signals are electrochemistry and spectroscopy.

Fig. 1 shows an example of an electrochemical detection mechanism, whereby electrical changes are detected based on chemical changes in the local environment of a sensing substrate.

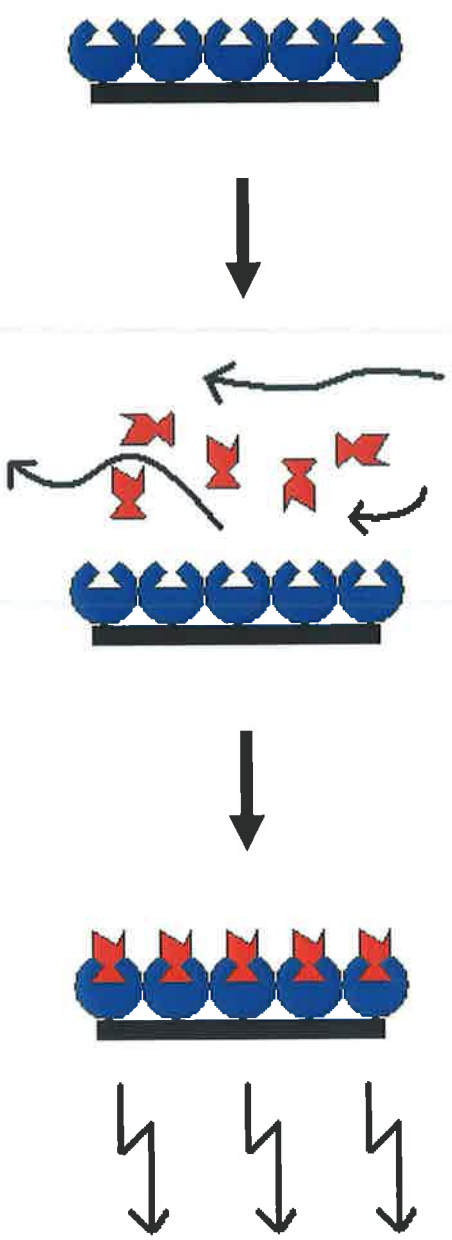

A layer of chemically-selective molecules are immobilised to the surface of a substrate.

The molecules are exposed to a solution, in which there are molecules to which the surface molecules preferentially bind.

Once the molecules have bound there is a change in the electrical signal, which can be detected trough an electrically-active substrate.

Fig. 1.1: *The schematic of a biosensor showing how an event on the molecular scale can be recognised due to a change in electrical signal. This signal can be thus converted to meaningful data (Such as a current response over time) by means of a transducer.*

From Fig. 1 it can be seen that a chemical reaction can be detected through analysis of an electrical signal, for example using amperometry whereby there is a current change in response to a binding event. This design can be used to determine the presence of particular chemicals, enzymes or antigens and can be used to determine the extent of the binding activity.

One example of a setup to do such is an ion-selective electrode (ISE) as this is capable of selectively identifying particular cations and anions. The analysis is in typically aqueous samples, which is important for environmental and clinical applications and usually requires no sample pre-processing. Within the Adaptive Sensors Group in Dublin City University numerous calixarene-based ionophores have been synthesised and incorporated onto ISEs, achieving good selectivity for cations such as sodium[1], lead[2], lithium[3] and mercury[4].

Advances in analytical systems to be deployed in the field include the remarkable advent of lab-on-a-chip (LOAC) devices. These miniaturised, portable devices include flow cells with pumps, valves, reagents and data transportation, offering complex analysis to be conducted remotely in the field.

Polymer membranes and surface films tend to be affected by exposure to the sample over time, so more robust designs need to be implemented with set internal calibration routines. If a sensor is subject to non-specific binding events the data received is unreliable and insignificant for deployment in the field.

Another area to exploit the wireless sensing potential is that of health diagnostics technology where such advances include smart fabrics where a sensor is integrated with the fabrics for the monitoring of such signs as breathing, heart rate and movement[5,6].

One idea to develop the concept of self-calibrating sensors is to implement a sensor that is capable of moving from an analysis environment to that of a calibrating one. Thus a low-power component that is capable of mechanically switching the location of a sensor is desirable, and one solution to this is through the usage of conducting polymer actuators. A device based on such materials would be capable of operating under very small voltages, while at the same time offering high force generation capabilities and power densities. The idea is based on the use of the actuator as a mediator and not as the sensor itself, so any attached sensing mechanism

must be lightweight so as not to inhibit the movement of the actuator to any large degree.

There are numerous issues to be dealt with concerning the implementation of calibration processes, not least the issue of a reproducible technique that does not itself suffer from a short lifetime.

Optical-based sensing systems include spectroscopic-based methods, such as absorption, fluorescence, phosphorescence and colorimetry. Hisamoto et al. have conducted absorption-based studies involving multi-information dyes[7]. Experiments conducted involved the use of one such dye for the detection of water content in an organic solvent whereby the detection is based on a shift in the maximum absorption of the dye. Fluorescence[8,9] and phosphorescence[10]-based studies have also been widely reviewed in the literature. Colorimetric techniques relate to responses whereby the signal is generated from chemically-induced colour changes over time. The techniques often relate to LED-based systems where a photodetector is employed in either a reflectance or transmission-based configuration.

One example of a colorimetric fluorescence sensor involves its use in the design of a dissolved oxygen sensor based on the quenching of a fluorescent compound[11-13]. This principle is based on the fluorescence of a ruthenium complex that strongly absorbs light in the blue regions of the spectrum. As the emission spectrum of ruthenium lies in the orange region of the spectrum there is only a small degree of overlap between the excitation source and the fluorescence emission, which can be modified effectively by the use of a filter rendering the excitation light getting through to the detector as effectively zero. In the presence of oxygen the fluorescence of the ruthenium is quenched, so a decreasing signal corresponds to an increase in the oxygen presence. This principle develops applications towards the design of dissolved oxygen probes for use in wastewater management. Similar techniques have been applied to the detection of carbon dioxide, again using a fluorescent-based dye, towards applications in multi-analyte detection systems and food packaging analysis[14-16].

The basic concept behind the LED-based colorimetric sensor is that there is an emission LED that will serve to emit light and a photodetector to receive the signal, be it a direct or reflected light source. A novel approach incorporating two LEDs, one acting as an emitter and the other operated in reverse bias to act as a photodetector has

been reported by Lau et al[17]. This concept has advantages in the simplicity of the setup and in the cost of production. There are two principle configurations that can be employed using such a design, the first is to set the LEDs directly opposite to one another so that the signal is generated from a translucent measurement substrate being moved between the two, still allowing transmission of the light through to the detector. The second configuration involves setting the two LEDs on the same side of the substrate so that the emitted light is reflected off the substrate and picked up by the photodetector. Both of these designs suffer from interference from ambient light, which can be combated by, especially in a flow cell setup, the encasing of the sensing component from outside light sources[18].

The basic concept involved in the development of these sensors has been reported on numerous occasions, with publications on dual transducer systems[19], LED and light dependent resistor (LDR) emitter/detector systems[20] and LED/photodiode systems[21]. Optical fibres have also been adapted to chemical sensing[22,23].

1.2 Chemical Sensing and Wireless Communications

Modern times have witnessed a revolution in the role of communications technology. The rapid development of the Internet into the global phenomenon it is now is represented by the fact that more and more business, both commercial and private is being conducted through it. It is a medium for people to control their finances (Internet banking), book flights and concert tickets, to organise business dealings (Video conferencing) or simply to stay in touch with friends (Email). With this wealth of information at our fingertips, and with the convenience of applying it to most designs, there has been considerable interest in the development of analytical science in conjunction with digital communications[24]. This is particularly relevant to environmental sensing where sensors are deployed in the field; a means for sufficient communication means that the sensor can be monitored without the need for physical examination of the device. Data assimilation can be achieved across a wireless network, and any discrepancies can be monitored autonomously. Moreover, groups of these sensors can be deployed in a given area, with the capacity to communicate with each other, giving a distribution of data, which is important for discerning how an environmental hazard could be spreading over the area.

Drift in analyte response and the deterioration of the sensitive interface are problems intrinsic to most chemical sensors. These issues are exacerbated in remote autonomous monitoring systems. A chemical sensor generally consists of a chemically-selective interface in or on a non-specific transducer. The interface is expected to selectively interact with the chemical species of interest and induce a change in either the optical or electronic properties[25]. Due to the variation between individual sensors and the material deterioration of the chemically selective interface over time, a calibration process is required to correct the output signal. However, calibration often involves the manual correction of sensor drift and can be time consuming, with regular calibrations rendering sensors unsuitable for long-term deployment in the field for environmental monitoring. Thus to develop a fully autonomous sensing platform it is highly desirable to implement a system that incorporates some form of self-calibration.

For the successful implementation of chemical sensors to the environment around us, a number of primary issues must be addressed. It is firstly imperative that

the sensors show the utmost reliability as they are to be deployed in the field and any incongruity would prove highly undesirable to correct regularly. In terms of a mass deployment philosophy the costs must be kept at a minimum, otherwise the sensors would not be economically viable. The cost of materials can be kept to a minimum through the use of inexpensive components such as LEDs, and the applications of very low power sources. The key issue with chemical sensors is their long-term efficiency as the sensor interface can have a propensity to degrade over time.

At its heart an automated sensor must contain a reliable sensor component, capable of reliably indicating the presence of a certain subject material. Around this sensor there must be a few further components. The data must be reliably transferred from the sensor to a source where it can be interpreted; one such source for this is through the advent of wireless communication. By using a network of chemical sensors operating across an area, it also offers the possibility to deduce whether one sensor is malfunctioning should it be out of sync with the others or offer a means of tracking the spread of a chemical species through the area. An example of the mass deployment of sensors across an area in a kind of network has been demonstrated by a team from Berkley who have developed a 50-node sensor network for the monitoring of seismic activity[26]. They have also demonstrated a 32-node sensor network, linked by satellite communication, which has been employed to study microclimates associated with the nesting sites of storm petrels[27].

Arora et al[28] have outlined the biggest current deployment of a WSN with respect to sensor nodes and the area covered. The central idea behind the project was to deploy a dense wireless sensor network that would be a virtual "tripwire" over a large area. The WSN would detect, track and categorise "intruders" that enter the area covered by the network. The project involved two demonstrations with the first comprising 90 Mica2 motes that were deployed over a 25 m x 10 m grassy area. The second used over 1000 'XSM' motes as sensor nodes and 300 'XSS' gateway motes.

1.3 *Inherently Conducting Polymers (ICPs)*

1.3.1 Background

Inherently conducting polymers (ICPs) in the contemporary sense are derived from the Nobel Prize winning discovery in 1977 by Alan J. Heeger, Alan G. MacDiarmid and Hideki Shirakawa concerning conductivity in polyacetylene[29]. Moreover it was noted that the doping of said films with controlled halogen concentrations further increased the electrical conductivity[30]. Through careful control of the doping process it is possible to vary the conductivity over a range of eleven orders of magnitude.

Further studies on the trans-$(CH)_x$ and cis-$(CH)_x$ isomers revealed scope for even higher conductivities[31]. Conductivity of polyacetylene films has been measured to as high as 10^5 cm^{-1}, almost as high as that of copper[32]. Other ICPs with a similar π-conjugated structure have been developed, in particular polypyrrole, polyaniline and polythiophene.

ICPs have many uses, among which is their potential for use in chemical sensing. Their electronic and mechanical properties offer a versatile sensing mechanism regarding composition, physical form and the nature of the analyte to be detected.

In the case of polypyrrole, which was first synthesised by Diaz et al.[33], the polymer is synthesised through electropolymerisation where pyrrole monomers are oxidised at an anode through the application of an external potential. The potential creates an insoluble film on the anode through a process shown in Figure 2.

Figure 1.2: Oxidation of pyrrole to polypyrrole. The counterion A^- is required to balance the charge on the polymer backbone, n=3-4 pyrrole units and m relates to the polymer chain length.

The counterion is important because it is incorporated to the polypyrrole matrix in order to balance a charge on the polymer backbone. The concentration of these counterions is high, and they are usually contained between planes of polypyrrole[34]. Ideally the polypyrrole would have alternating rings, with one facing up and the next facing down, to give symmetrical planes throughout, between which the counterions are located[35]. Distortion of this ideal is seen in real terms though through crosslinking events[36].

The first step in the polymerisation process is monomer oxidation, followed by a radical-radical coupling mechanism. Studies by Andrieux et al. have concluded that the electropolymerisation of polypyrrole is based on cation radicals that are formed, and subsequently couple together[37]. The natural repulsion of the radicals is assumed to be counteracted by such media as the solvent and the counterion, hence chain growth continues until the charge necessitates the incorporation of a counterion. Upon reaching a critical chain length, the solubility limit is reached and the polymer precipitates on the electrode surface.

Polymerisation is able to progress quicker once there is a layer of polypyrrole deposited on the anode, and will continue until the reaction is brought to an end. The experimental conditions are of vital importance as they influence the rate of growth and quality of the resultant film. Electrochemical conditions such as the potential difference and applied current are important to ensure that the film is deposited in the first place and that overoxidation doesn't occur, which will result in unresponsive films. The solvent used relies on being able to solvate the electrolyte salt, while at the same time not inhibiting the polymerisation through reacting with the intermediate

radical species. A non-nucleophilic solvent is essential to meet these requirements, whilst bubbling the solution under nitrogen before polymerisation can help to rid the system of dissolved oxygen, which may also promote radical interference. The electrode material and counterion employed are also critical to the desired polymer output, and the interactions of all the abovementioned factors need also be considered, as they influence the rate of reaction[38].

In terms of the electrochemical cell used for the synthesis, the counter electrode must be positioned effectively, in that the electric field generated from it dictates the even growth of the polymer. To this end a concentric-style counter electrode was used, to provide similar deposition across the entire film. A two-electrode approach can complicate control of the potential but in galvanostatic mode this is not as important as the potential changes while the current is applied. The iR drop can also be an issue in this respect as the electrode resistance increases as more polymer is deposited.

Another factor influencing polymer growth is the temperature of the cell. Higher temperatures can accentuate unwanted side reactions, involving the reaction of oxygen with the radical species. Conducting polymer synthesis at low temperatures can combat this, as it has been shown that this method produces more conductive films[39].

1.3.2 ICP Actuators

One useful and variable application of ICPs is how they can be used to convert electrical energy to mechanical energy through the advent of electromechanical actuators, or artificial muscles[40]. The principal upon which such an actuator operates is that the material of which it is composed changes physical dimensions under electrical stimuli. For ICPs this is related to the induced volume change upon oxidation and reduction of polymer films, whereby ions move into and out of the polymer[41]. High volume changes have been reported on very small devices, and favourable responses have been noted for ICP actuators when comparing stress values with those of natural muscles[42] and piezoelectric polymers[43]. One of the principle advantages that the ICPs have over their piezoelectric counterparts is their low operating voltage, which is on the order of 1-2V, compared to 100-200V.

The films can then be configured in such a way that an electromechanical actuator device can be developed from it. This can be achieved by taking a sheet of a porous material and sputter-coating a conducting surface such as gold on either side before depositing a film of the ICP on either side. Both sides of the film are electrically insulated from one another and with the presence of an electrolyte solution volume-changes can be induced through application of a potential across the films. Oxidation of one side of the material results in anion intercalation within the film from the electrolyte, while the other side is being reduced, causing a swelling of one side of the actuator and resulting in a bending to one side. Switching of the potential causes the film to become reduced with the anions being expelled to the other side of the film where the polymer has become oxidised, resulting in a counter-bending effect. This switchable response has spawned numerous applications, including a novel approach into research for the development of cochlear implants[44].

Research into actuators based on ICPs is still very much in its infancy as other materials that have been used in actuation mechanisms have been in use for over half a century. This does, however, offer a means upon which to evaluate the performance parameters of ICP-based models.

One benefit of the ICPs is their ability to be operated at very low voltages. This property is demonstrated in comparison to the piezoelectric polymer poly(vinylidine fluoride), which gives a 0.1% dimensional change for a micron-thick film at 30V. ICPs are capable of 10% dimensional changes under only a couple of volts[45]. ICP actuators also display a greater stress generation capacity compared to the piezoelectric polymer, and the work per electrochemical cycle and the mechanical failure stress can far exceed[40].

One of the disadvantages of using ICP actuators is that it is difficult to control the precise positioning of the actuator. While the actuator can be maintained at a particular position, at equilibrium, without consuming energy it can suffer positional drift through, for example, electrode dopant redistribution. Suggestions to control this include the use of a mechanical stopper device or to employ some form of feedback loop to control the voltage[40].

Another issue is that the response is dependent on molecular diffusion and hence the speed of the response is dictated by the thickness of the films. The response of thinner films also suffers limitations, though this can due to resistive effects in the electrolyte. Much research has been done into the switching times for ICPs and fast

times have been recorded[46]. Also, doping and de-doping in ICPs is not entirely reversible, which duly affects the lifetime of the polymer though lifetimes have been reported at 10^6 cycles for polymers in electrochemical displays[47,48].

Polypyrrole-based actuators[49-52] have become increasingly studied due to their favourable mechanical properties of high stress and strain values, in particular when subjected to an external load[53]. By increasing the external load, there is found to be a linear decrease in the rate of strain. This is an important factor in the application of ICP actuators to chemical sensing as any component attached to a film must be as lightweight and as non-intrusive as possible. Because of their dependence on an electrolyte solution to facilitate the diffusion of anions necessary for actuation, operation in solution has always been much easier to accomplish than in air. However progress has been made and actuators have now been developed that display stresses comparable with those of mammalian muscle[42,54], promising much in the field of biomimetics.

One of the major issues associated with applying ICP actuators to anything has been the lifetime associated with the device in operation. Because of the dependence on a (usually) liquid electrolyte there are always issues associated with evaporation and degradation of the polymer due to nucleophilic attack. One potential solution has been the advent of ionic liquid electrolytes[55], which tend to be very stable and show negligible evaporation. Studies conducted on polypyrrole actuators comparing the lifetimes of an organic electrolyte to an ionic liquid electrolyte showed the former to degrade after about 2000 electrochemical cycles, while the ionic liquid showed only a 17% decrease in displacement after 6000 cycles.

One application of a polypyrrole-based actuator to a sensing system has been reported by Andrews *et al.* whereby the actuator is used as a valve in the storage of fruit[56]. Because apples store best in an environment of about 5% oxygen a system has been developed where the oxygen is measured by a zinc-based air cell[57] and the entry of gas is regulated by the actuator. The actuator showed reliable and repeatable behaviour for about 50 hours before deteriorating due to the evaporation of liquid electrolyte.

A number of projects have been undertaken in the Intelligent Polymer Research Institute (IPRI) in Wollongong, Australia[43]. One such project involves the development of a rehabilitation glove, based on a concept by De Rossi[58] of the

University of Pisa, Italy, where the actuators are incorporated into the glove to aid rehabilitation through assisted movement.

Another project IPRI are involved in is the use of actuators in systems for electronic Braille screens. The concept is based on low-cost, refreshable surfaces where the actuators are used through electronic stimuli to raise and lower the Braille dots.

1.3.3 ICPs in Chemical Sensing

ICPs also have many applications in chemical and biological sensors[59]. Chemical sensing is based primarily on the detection of certain analyte materials and this is achieved through specific interactions on the molecular level. Through a chemical or biochemical reaction or response a signal is generated and it is the efficient and applied transduction of this signal that is important in defining the sensitivity and selectivity of the sensor.

The most common means of analysis when dealing with chemical sensors are through electrochemical responses and through optical measurements. Common types of electrochemical measurements involve voltammetry, resistometry and amperometry. Voltametric-based sensors have appeared recently in the literature. Reisberg et al. have developed an electrochemical DNA sensor whereby the electrode is coated with a conducting polymer film[60]. The electrode is used for the chemical detection of oligonucleotide hybridisation, where changes in a square wave voltammetry signal are attributed to this hybridisation though correlation with quantitative fluorescence spectroscopy. Barisci et al. have investigated the potential of using an array of sensors, derived from electrochemically derived ICP films, to develop an 'electrical nose' sensor[61]. The electronic nose concept has been discussed previously and has received considerable interest in sensor research towards environmental monitoring[62]. Using polypyrrole films, instilled with a range of dopants to examine the selectivity of the films, sensors were developed for the detection, identification and quantification of a range of volatile aromatic hydrocarbons such as the BTEX quartet of benzene, toluene ethyl benzene and xylene. The detection system was facilitated using changes in the film's electrical resistance.

Nguyen et al. have further developed this idea towards the production of low-cost disposable sensors based on screen-printed electrodes[63]. While not as sensitive to

organic vapours as conventional gold-based substrates, acceptable reproducibility has been noted for the concept.

Ngamna et al. have presented a biosensor with the detection method based on the amperometric response of the ICP poly (2-methoxyaniline-5-sulfonic acid) (PMAS)[64]. The device essentially consists of a base electrode, in this case indium tin oxide (ITO), which is coated in a mediator material that serves as a substrate on which to immobilise a sensitive biomolecule species. For this research the PMAS served as the mediator upon which horseradish peroxidase (HRP) was immobilised. Subsequent interaction of the HRP with hydrogen peroxide (H_2O_2) causes a measurable amperometric response. H_2O_2 detection is important in a number of fields, for example in the organic oxidation of harmful products like BTEX pesticides (with catalysis), or in toxicity reduction where, again with catalysis, organics are chemically broken down into smaller, less toxic and more biodegradable fragments.

1.4 pH Sensing

pH-sensitive dyes such as bromocresol green have frequently been applied to chemical sensing. Such dyes can operate within the visible spectrum whereby they can be easily monitored by employing a colorimeter system. Pacquit et al. have applied these components towards the development of a sensor for the detection of food spoilage in fish[65]. The dyes are used as a "chemical barcode" to detect the volatile components of amines and ammonia.

The pH sensitive dyes operate on the principal of chemical changes occurring upon their introduction to differing pH environments. In acidic media a protonated form of the dye is activated as the acid donates protons, which are incorporated to the dye, resulting in a particular coloured form of the dye. The opposite is true in basic media as the deprotonated form becomes dominant due to the protons being taken from the dye, and a concomitant colour change is observed. These changes occur around the point of their acid ionisation constant, or pK_a, which is the point at which the protonated and deprotonated forms exist in the dye in equal measure.

The equilibrium constant of a weak acid in aqueous solution is called an acid ionisation constant, or K_a. In any dissociation a weak acid can be separated into its component ions, consisting of its conjugate base and a proton.

$$HA\ (aq) \rightleftharpoons H^+\ (aq) + A^-\ (aq)$$

The K_a of the equilibrium is thus

$$K_a = \frac{[H^+][A^-]}{[HA]}$$

and when the acid is 50% dissociated, then $[A^-] = [HA]$ and the $K_a = [H^+]$. The pK_a at this point is thus equal to the pH.

The application of bromocresol green dye, and also of a number of other dyes based on a similar formulation, is discussed in this work. The dyes are fixed to the actuators to generate a model capable of moving the sensor into the sensing environment. Changes in the colours of the dyes can then be monitored before the

actuator can relocate the sensor to a re-calibration point. The pK_a can be determined from the change in colour of the dyes across a pH range, as will be discussed in Section 3.4.2.

Similar pH-sensing materials have been used in colorimetric-based sensors developed in the Adaptive Sensors Group in Dublin City University. The colorimetric sensing is based on the aforementioned dual emitter/detector LED setup, and a range of solute dyes are used as the sensitive materials[17,66]. The work has demonstrated how the combination of a low-cost, low-powered LED system can be used to achieve high sensitivity pH measurements. O'Toole et al. also demonstrated that the system was capable of determining the pKa of the bromocresol dye through analysis over a range of pH values[66]. Badugu et al. have developed probes based on boronic acid and its affinity in binding with strong bases, whereby the responses show spectral shifts and intensity changes with pH[67].

2. Experimental

2.1 Materials and Methods

Polyvinylindene fluoride membrane (PVDF, Millipore) with ~ 110 μm thickness and average pore size ~ 0.45 μm was used as received without additional treatment. Pyrrole (Merck) was distilled and stored under nitrogen at ~ –20 °C before use. Propylene carbonate (PC) (Aldrich), tetrabutylammonium hexafluorophosphate ($TBA.PF_6$) (Aldrich), bistrifluoromethanesulfonimide lithium salt (LiTFSI) (Fluka), 1-butanol (Riedel-de Haën), acetone (Aldrich), acetic acid (Aldrich) and aqueous ammonia solution (30%) (BDH Laboratory Supplies) were used without further purification. The Bromocresol green, bromocresol purple, m-cresol purple and bromothymol blue dyes were all acquired from Sigma Aldrich, as was ethyl cellulose and tetraoctylammonium bromide (TOABr).

Instruments used for the actuator synthesis were the Uniscan Instruments PG580 Potentiostat/Galvanostat in Dublin City University (DCU) and the EG&G Princeton Applied Research Model 363 Potentiostat/Galvanostat in the University of Wollongong (UoW), while for analysis of the actuator properties the Solartron 1285 Potentiostat was employed. Sputter coating was carried out in DCU on the Polaron SC7640 Instrument distributed by Quorum Technologies and on a Dynavac sputter coater in UoW.

2.2 Preparation of Dyes

A procedure for the preparation of the dyes was followed in each of the sensor fabrications. The dye formulation was developed in-house for use in amine sensing for food spoilage[65]. The preparative steps begin with the solvent, which through optimisation experiments have shown a 2:1 v/v 1-butanol/acetone solution to be desirable. The next step is the addition of the salt, in this case tetraoctylammonium bromide (TOABr), followed by the dye. These are added first to facilitate full

dissolution in the transparent butanol/acetone solvent before the titanium dioxide (TiO_2) was added, which served to give the dye an opaque appearance. The solution was sonicated after the TiO_2 addition to fully dissolve the solution before the polymer material (Ethyl cellulose) was added, as this made the solvent viscous, which made dispersal of any subsequent materials difficult. The solution was then sonicated for 3-4 hours to accommodate full dissolution of the ethyl cellulose. The molar ratio of the TOABr to the dye was approximately 2.6:1 as this limits the effects of leaching of the dye when it is applied to a substrate, particularly if the dye is to be used in solution-based analysis.

3. Results And Discussion

3.1 Film Synthesis

3.1.1 Preparation of Actuators

The polypyrrole films were galvanostatically synthesised onto porous membranes of polyvinylidene fluoride (PVDF). Solutions of 0.05M tetrabutylammonium hexafluorophosphate ($TBA.PF_6$) or Lithium bis(trifluoromethansulphonyl)imide (LiTFSI) were prepared in propylene carbonate and a 0.06M solution of pyrrole monomer was made up in this prior to synthesis. A 0.5% (w/w) aliquot of water was also added to avoid pyrrole protonation and chemical polymerisation around the electrode[68]. The solution was placed under nitrogen gas for ten minutes to purge oxygen from the system before being added to a custom-designed two-electrode cell. A large stainless-steel mesh was lined around the inside of the cell to act as the counter electrode while the working electrode was composed of a $5x6cm^2$ gold-coated PVDF membrane. The membrane is used to facilitate ion transport back and forth between the two sides of the film during redox processes. The gold substrate was sputter-coated onto the PVDF membrane before the entire cell setup was placed in a freezer at –20°C and the polymerisation of pyrrole was carried out galvanostatically on both sides of the membrane at a current density of $0.1mA/cm^2$ over 12 hours. This typically results in a film thickness of about 30μm being obtained[56]. The polypyrrole was then cut into a strip of 5 x 1cm dimensions and a sensing tip was applied to one end.

Synthesis of polypyrrole films is carried out over time at a positive oxidation potential, which varies due to the constant current applied. The monomer pyrrole units become oxidised and form polymer chains, which when exceeding a certain length come out of solution and deposit on the working electrode surface. A positive charge is thus induced on the backbone during the oxidation process, and this requires the activity of counterions to neutralise the charge and to stabilise the polymer. This movement of ions becomes particularly relevant when concerning the method of ionic diffusion involved in the actuation process. Anionic diffusion occurs when the anion is of sufficient size and mobility to move freely through the polymer, while cationic diffusion predominates when anionic movement is slow or the anion is too large,

instead becoming trapped within the polypyrrole matrix. In the case of the two electrolyte materials mentioned, TBA.PF_6 and LiTFSI, anionic diffusion has been shown to be predominant, with the TFSI-based films showing a faster charging than the PF_6 films, despite showing lower conductivity[69]. Because of the faster anion movement there is a greater film actuation for a given time period.

The actuation of the polymer is described through application of a potential difference across the two sides of the film, as shown in Figure 3.1. This is possible as they are both electrically insulated from one another by the thin PVDF membrane that also facilitates ion movement. Electrochemical switching of the potential between ±1V results in a cyclical oxidation and reduction of the films, relative to one another. This means that during reduction the TFSI anion diffuses out of the polymer due to a neutral charge being induced on the polymer backbone, shown in Fig. 3.2 (a). An associated contraction of the film occurs with the anions diffusing through the porous intermediate membrane. This process is accelerated by the oxidation process occurring in the film (shown in Fig. 3.2) on the opposite side of the actuator, whereby the backbone of the polymer becomes positively-charged, influencing a diffusion in of the anions. This anion movement is accompanied by that of the polar propylene carbonate solvent, which associates itself with the negative charge on the anion. The potential switching across the actuator thus induces a volume switching between the two polymer films, initiating the expansion and contraction of the actuator. The actuator will bend in the directions shown in Figure 3.1 as a result. Switching the potential will result in a reversal in the ion diffusion and the actuator will begin to bend in the opposite direction. The diagram in Figure 3.2 shows the stages that occur with respect to the oxidation state of the polymer[70]. Fig. 3.2(a) respresents the neutral form of polypyrrole, while oxidation results in a polaron (Fig. 3.2(b)), where the removed electron causes a positive charge on one of the pyrrole rings. An unpaired spin is also formed, and under further oxidation a bipolaron is formed (Fig. 3.2(c)) as this formation is energetically favoured to the formation of two separate polarons[70]. This charge occurs over about four pyrrole rings, and the movement of anions in the polymer actuator is associated with the positive charges on the polymer in this state.

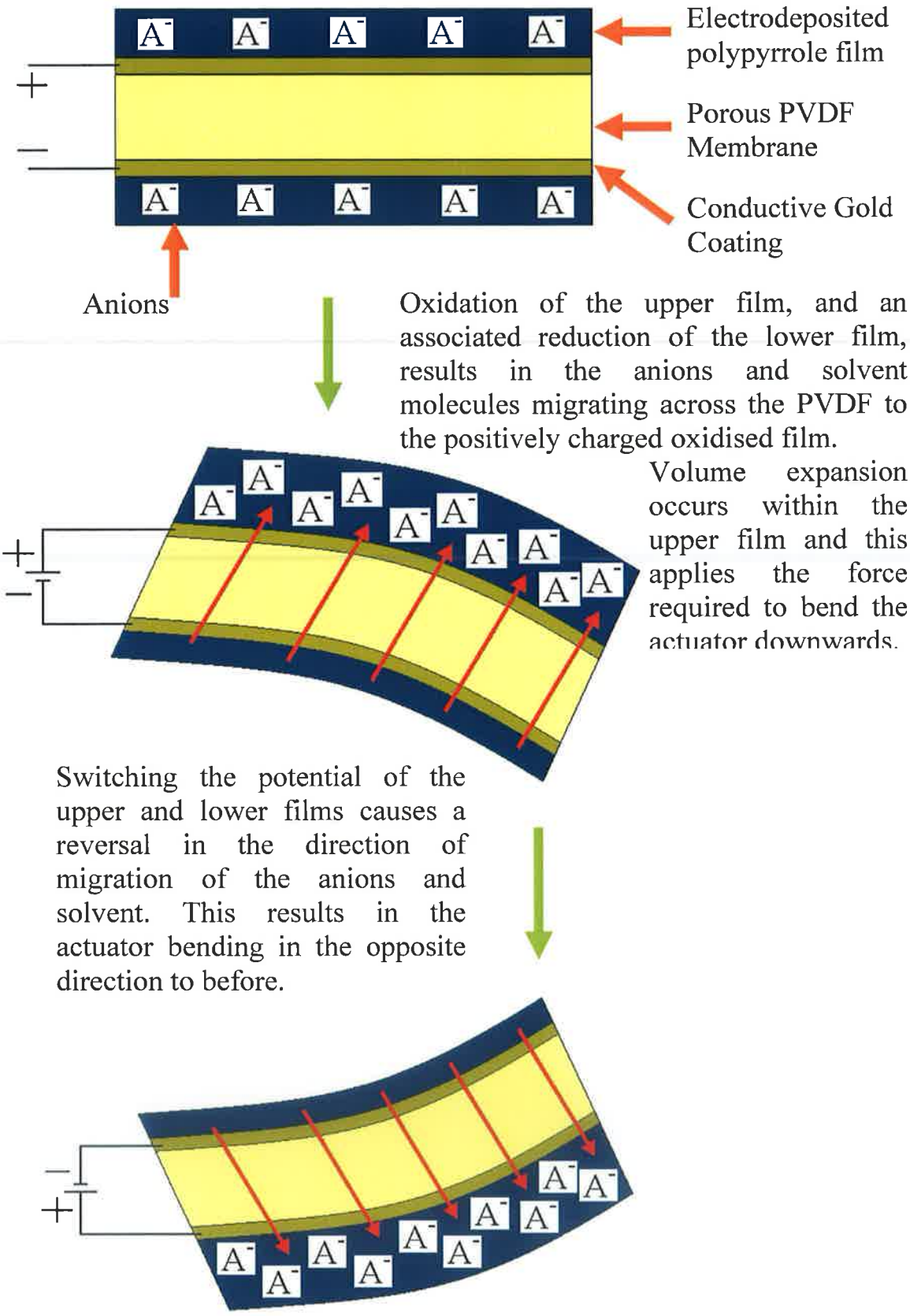

Figure 3.1: Schematic of actuator operation. Control of the potential initiates movement of anions from the reduced to the oxidised film.

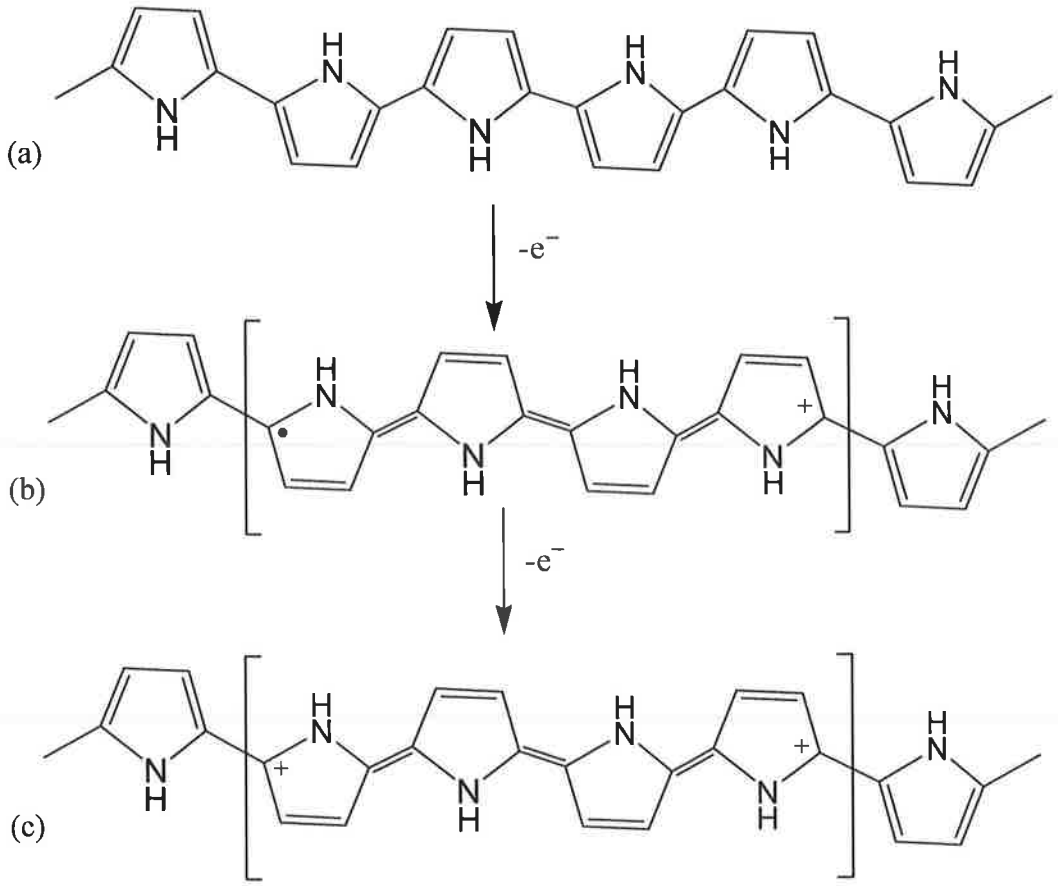

Figure 3.2: The conductivity of polypyrrole films is linked to the π-conjugated backbone structure of the polymer[71], which is associated with the double bonding across the chain. In the reduced form there is no charge on the backbone (a) but when the polymer is oxidised, a removal of one electron creates a polaron (b) whereby there is one positive charge and an unpaired spin. Further oxidation results in the removal of a further electron and the creation of a bipolaron (c). Because of these induced charges on the chain, counterions become associated to counteract this charge, thereby increasing the volume of the polymer. The polarons and bipolarons act as the charge carriers, through the rearrangement of double bonds across the polymer chains[71]. The mobility of these carriers directly influences the conductivity, and is based on interchain and intrachain components. Intrachain charge transfer occurs where there are crosslinking defects in the planar nature of the chains, and the charges can move between adjacent planar chains.

3.1.2 Constant Current Method for Polypyrrole Film Synthesis

The actuators were fabricated from a porous membrane, coated in a thin conductive layer to facilitate the electrodeposition of the polypyrrole. The porous membrane was a thin film of PVDF, with a pore size of 0.45μm to allow the transport of ions. The conductive layer was provided through the sputter-coating of gold or platinum to each side of the PVDF. It was upon this substrate that the polypyrrole was grown.

The films were grown galvanostatically, whereby the current was held constant over a set period of time and the voltage was measured with respect to this. The parameters employed to the growth of the films were to use a $0.1mA/cm^2$ current density across the film, for a time period of 12 hours to facilitate an adequate film thickness for polymer actuation[41]. In the case examined below a film of dimensions 6.3 x 5cm was used, yielding an area of $63cm^2$ when both sides of the substrate were taken into account. This area, along with the desired current density, requires that a 6.3mA current be applied across the film for the duration of the 12 hours.

The electrochemical setup consisted of a two electrode cell where the working electrode is the film itself and the counter electrode is used as the reference electrode, in this case a wire mesh wrapped around the inside of the cell to maximise area and maintain a steady signal. Because the current is being maintained at a constant 6.3mA the potential varies slightly, beginning at about +2V and rising gradually to about +4V by the end of the deposition. This is due to bubbles forming on the surface of the counter electrode, whereby the surface area is diminished, along with the charge being passed for deposition of the polymer. In order for the current to remain constant at the working electrode, and hence the polymer deposition, the potential is increased to compensate for the effect. More bubbles form as the deposition process continues and there is thus a continuous increase in the potential over the duration. The application of the constant current for twelve hours results in a charge of 270C being passed across the film. This corresponds to the theoretical expectation where the charge is calculated from the time (43200 seconds) multiplied by the current applied. The current applied can be derived from the current density ($0.1mA/cm^2$) multiplied by the area of the film surface ($63cm^2$). After 7 hours, for example, as shown in Figure 3.3, the charge is measured to be at 159.38C, which corresponds to theoretical expectations.

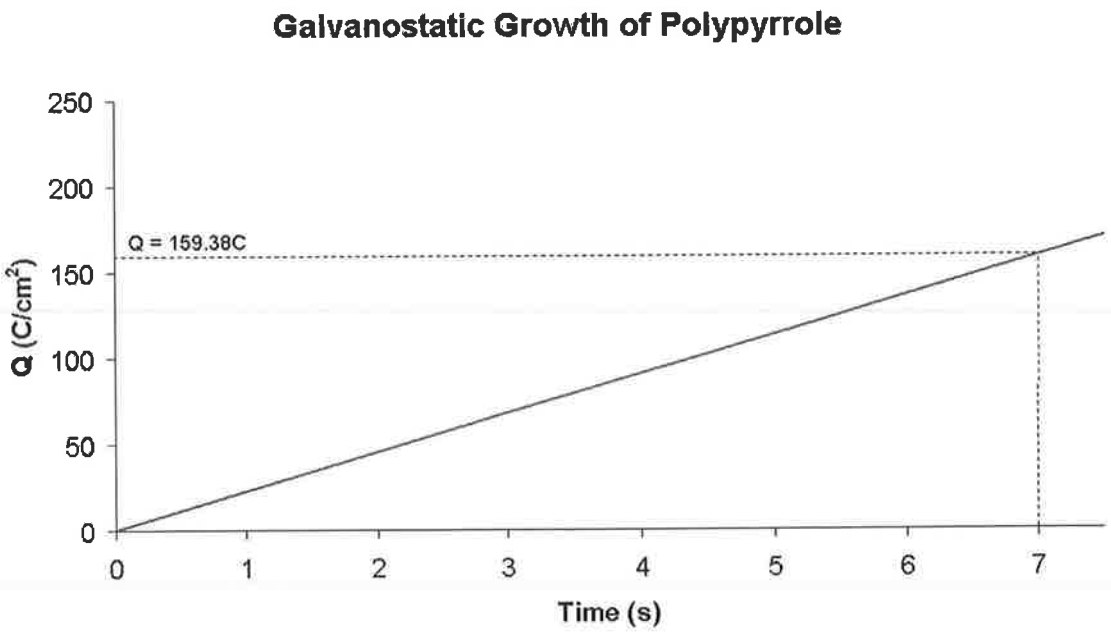

Figure 3.3: Graph showing the charge against time for the galvanostatic growth of the polypyrrole.

3.2 *Electrochemical Characterisation*

3.2.1 Power and Energy Analysis

The waveforms shown below in Figure 3.4 depict the applied voltage and the resultant current response associated with the actuation of the films over a five-cycle period. The films were run between an oxidation potential of +1V (point a) and a reduction potential of –1V (point c). Cyclic voltammetry was used to apply a triangular voltage waveform, which meant that there was a slower gradient of electroactivity within the film than would be seen using a squarewave signal. This gave a steady diffusion of ions between the two sides of the films and allows more control of the position of the actuator. In contrast, squarewave signals involve an almost instantaneous switching between the oxidation and reduction potentials, meaning that the bulk of the ion movement occurs within this transition and that there is a very rapid movement of the actuator. The cyclic voltammetry method was generally preferred, particularly in the video analysis techniques mentioned later, as the sensor response could be easily tracked and measured across the entire cycle.

The current responses are periodic and show a sharp change in signal upon voltage switching. This is due to the large initial change in anion concentration within the films. Under oxidation, the anions are attracted in to the positive charge initiated on the polymer backbone (Figure 3.2). Under reduced conditions the concentration of anions decreases due to the neutral charge induced on the polymer, and the resistance becomes larger, resulting in a decrease of current. The opposite occurs upon subsequent oxidation of the film.

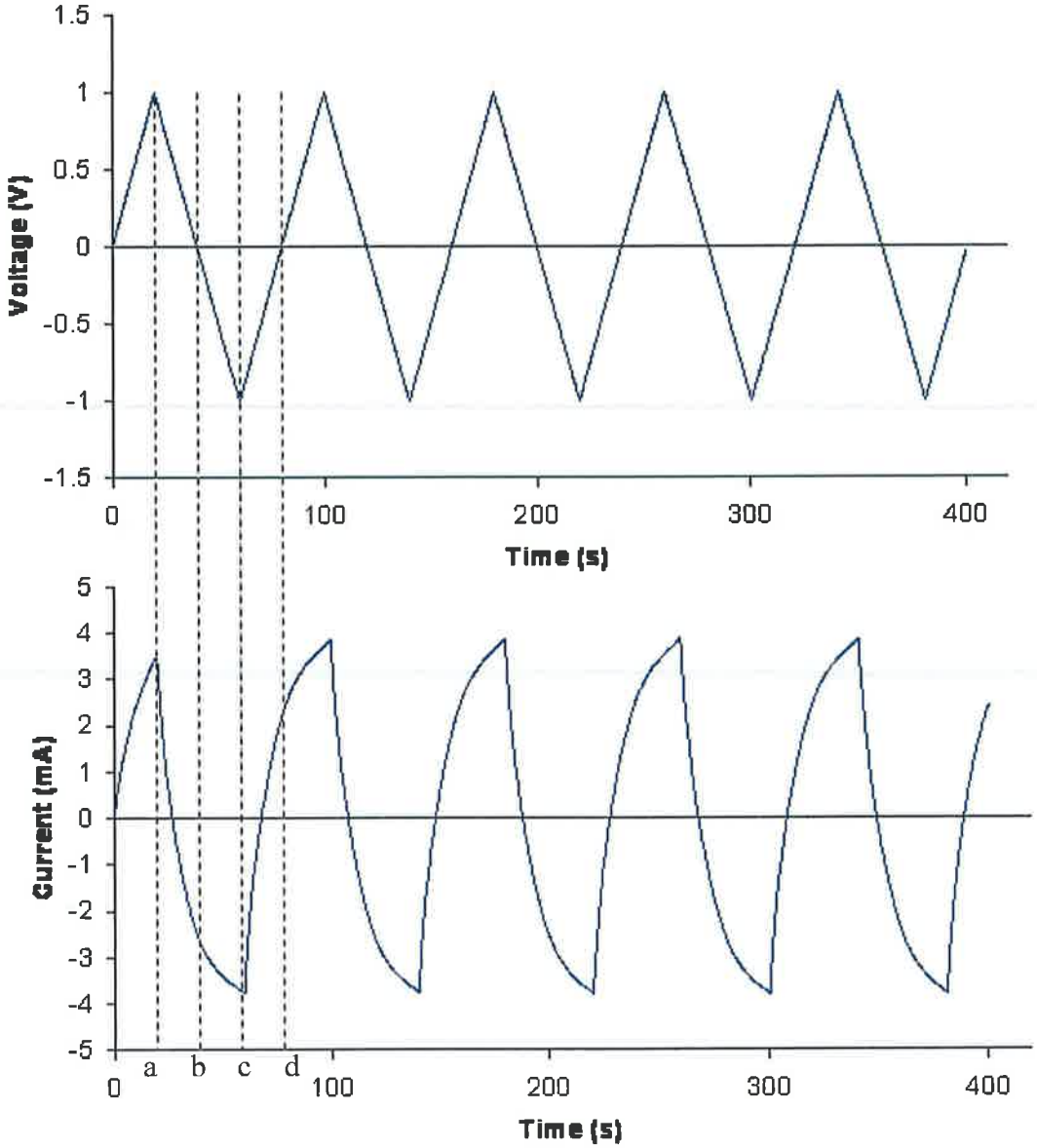

Figure 3.4: The cyclic voltammetry wavesignal with respect to the voltage applied and the current response. The dotted lines trace the current response at specific potentials; at +1V (a), 0V (b), -1V (c) and back to 0V (d) again.

From Figure 3.4 it can be seen that the current response at the +1V potential (point a) is also at a peak. At zero potential (points b and d) the current does not correspond to zero current however, due to a discharge in the polymer, caused by a capacitive effect whereby the polymer stores charge[41]. This effect is seen each time the polymer actuator is switched, and corresponds to a negative power consumption, as is seen in the diagram below.

The data from Figure 3.4 can be used to plot the power distribution of the actuation over time, using the relationship between power, current and voltage given by P=IV. The negative power segments correspond to negative current responses at positive potentials, or vice versa. This occurs because the current is being delivered from the actuator to the potentiostat, due to the discharge effect described above.

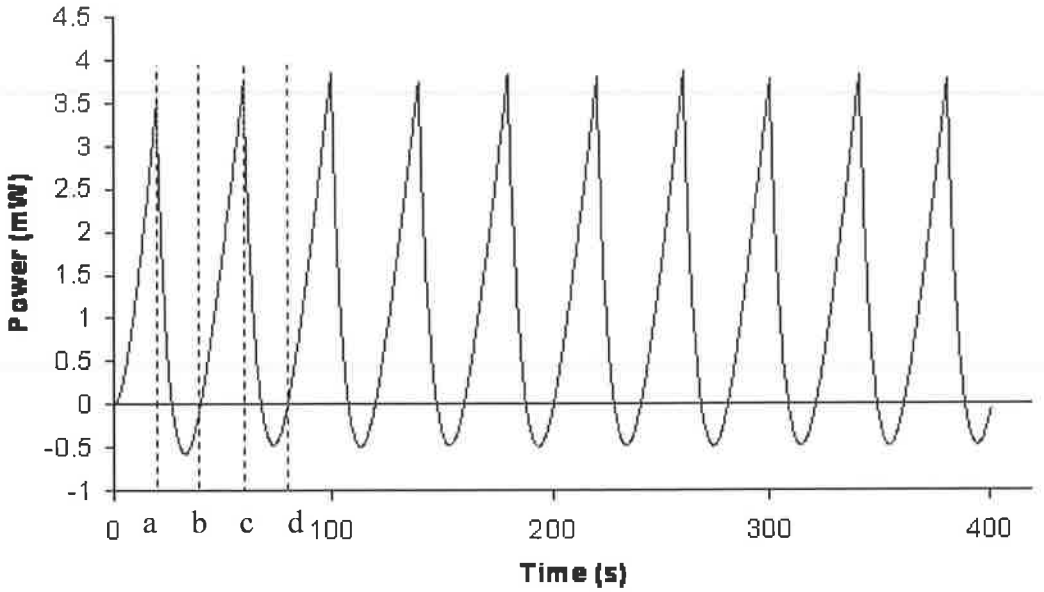

Figure 3.5: Graph showing the positive power distribution over time. The dotted lines again represent the points corresponding to +1V (a), 0V (b), -1V (c) and 0V (d) respectively.

It can be seen in Figure 3.5 that the power maxima correspond to the potential maxima (points a and c); this is when the most power is being drawn from the potentiostat. At zero potential (b and d) there is, of course, zero power being drawn.

Cycle Number	1		2		3		4		5	
Redox Status	Ox.	Red.	Ox.	Red.	Ox.	Red.	Ox.	Red.	Ox.	Red.
Voltage (V)	+1	-1	+1	-1	+1	-1	+1	-1	+1	-1
Current (mA)	3.51	-3.76	3.86	-3.76	3.86	-3.79	3.87	-3.79	3.86	-3.79
Power (mW/cm^2)	3.48	3.76	3.85	3.72	3.81	3.80	3.86	3.79	3.81	3.78

	Average		Standard Deviation	
Redox Status	Ox.	Red.	Ox.	Red.
Voltage (V)	1	-1	0	0
Current (mA)	3.79	-3.78	0.16	0.02
Power (mW/cm^2)	3.76	3.77	0.16	0.03

Table 3.1: The data showing the current, power and energy responses involved over five actuation cycles of the polypyrrole films.

The data above shows the relationship between the voltage, current and power during the five cycles. The voltage is switched between ±1V for the oxidation and reduction potentials respectively. The current and power peaks are seen to remain at almost constant values throughout, as is shown by the low standard deviation values. The actuator (typically on the order of $10cm^2$) operates on the order of mW/cm^2, which shows its potential for low-power operations, ideal for the development of low-cost sensing techniques.

3.2.2 Strain Analysis

Strain is the ratio of the change in length of a material to its original length. It is a measure of deformation in the material due to the stress caused by external forces. In the case of the polypyrrole actuator the stress is due to the volume expansion caused by the electrically-induced migration of anions, and because of this the length of the film will increase slightly, causing the film to bend (See Figure 3.1).

This analysis was carried out using visual data over a 40-second cycle of the conducting polymer actuator, with the sensor head attached to the actuator tip. The images were captured at two-second intervals during the cyclic voltammetry cycle, between the potentials of ±1V. The strain indicates the extent of bending observed in the polypyrrole strip; the curvature of the strip was used to trace out a circle (See Figure 3.6) of which the radius (r) could then be calculated according to the formula

$$r = l/\theta \qquad \text{(Eqn. 3.1)}$$

where l is the arc length (in this case the 5cm long polypyrrole strip) and θ is the angle in radians. Using this formula, with θ being measured on a paper printout with a protractor, the radius of the imaginary circle could calculated over a range of actuator positions. From these values of circle radius, corresponding to the actuator at different potentials over the electrochemical cycle, the percentage strain could be calculated at these positions using Eqn. 3.2, which will now be derived.

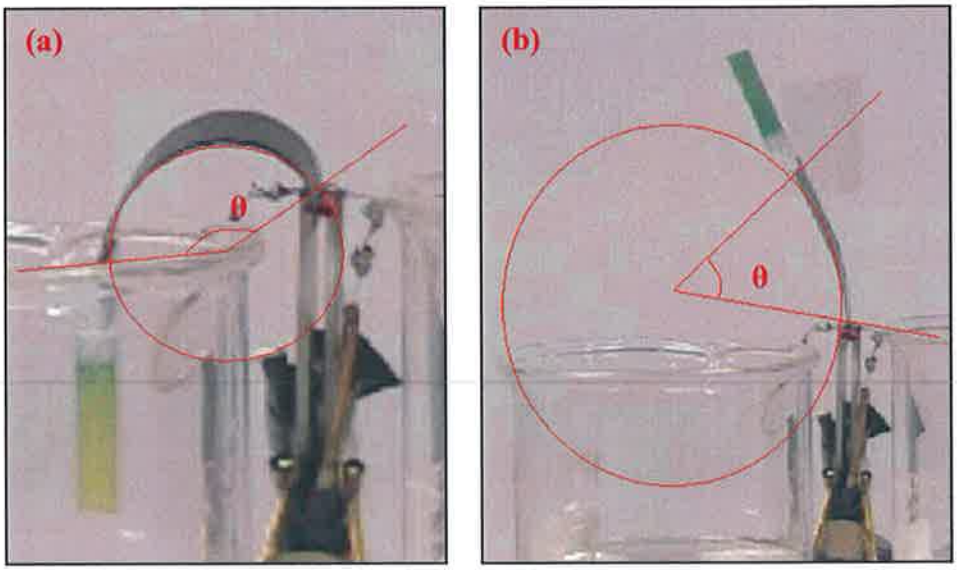

Figure 3.6: Radial analysis of the actuator. (a) was taken after 18 seconds and (b) after 30 seconds. In image (a) θ was estimated to be 166°, which upon using the strain formula below corresponded to a percentage value of 1.62%. In (b) θ was estimated at 33° with a resultant strain of 0.32%.

The mathematical definition of strain (S) is that it is the ratio of the change in length (Δl) of an object to its original length (l), as shown in Eqn. 3.2

$$S = \frac{\Delta l}{l} \qquad \text{(Eqn. 3.2)}$$

Take into account the following diagram:

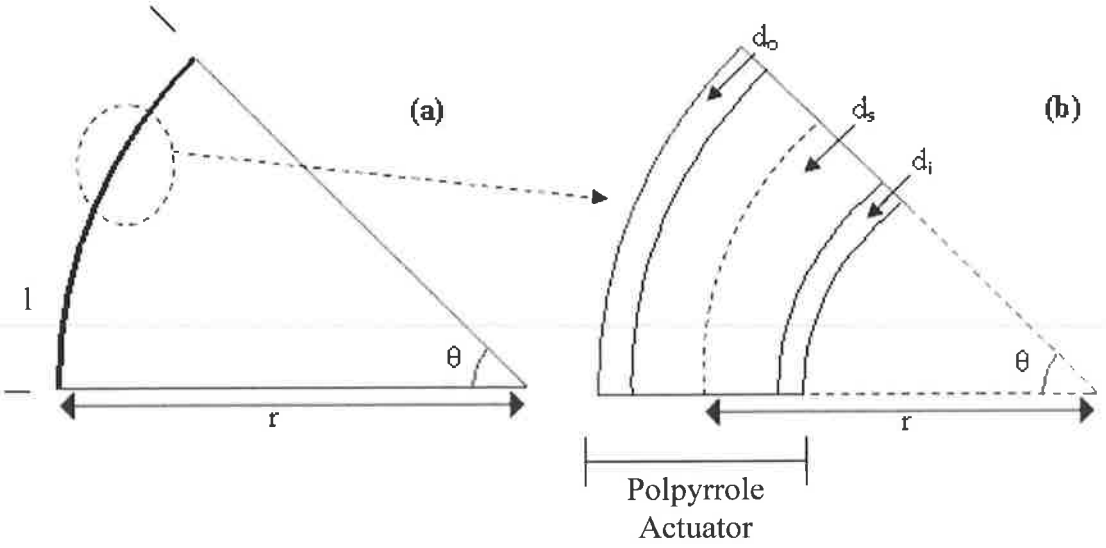

Figure 3.7: Diagram of the components of the strain calculations for the actuator.

The segment labelled (a) in Figure 3.7 shows the polypyrrole actuator denoted by the arc length l, which as it starts to bend spans an angle θ, defined by the radius r according to Eqn. 3.1. Segment (b) shows a more detailed representation of the laminar structure of a portion of the actuator shown in (a), whereby the thickness of the two films of polypyrrole are represented by d_o and d_i (The outer and inner films respectively) and d_s represents the thickness of the PVDF membrane. The radius r is calculated from Eqn. 3.1 according to the measured angle θ for any potential. In Figure 3.7 the radius is shown as the distance from the origin of the imaginary circle to the centre of the PVDF membrane, shown as the dotted line down through the centre of the d_s region. If we define this as the initial length of the membrane, then

$$l = r\,\theta.$$

If we take the outer film of polypyrrole (d_o), which has being subjected to the external stress and has expanded, the extra distance (x) from the centre of the PVDF membrane (dotted line through the d_s region) to the centre of the outer film can be calculated to be as follows

$$x = \frac{d_0 + d_s}{2} \qquad \text{(Eqn. 3.3)}$$

Therefore it can be derived that the length of the outer film (l_o) of the actuator at this point is as follow:

$$l_o = \left(r + \frac{d_o + d_s}{2} \right) \theta$$

Because the strain is defined as the ratio of the change in length to the original length the equations can be put together in the following form:

$$s = \frac{l_o - l}{l} \quad \Rightarrow \quad s = \frac{\left(r + \frac{d_o + d_s}{2} \right) \theta - r\theta}{r\theta} \quad \Rightarrow \quad s = \frac{d_o + d_s}{2r}$$

Thus the percentage strain is signified by the following formula[41]

$$s(\%) = \frac{(d_o + d_s) \times 10^{-4}}{2r} \times 100 \qquad \text{(Eqn. 3.2)}$$

where d_s is the thickness of the PVDF membrane and d_o is the thickness of the outer polypyrrole film. The 10^{-4} is a conversion factor from μm to cm. The thickness of an expanded (oxidised) polypyrrole film has been experimentally measured in the University of Wollongong to be 30μm, corresponding to the 12-hour period over which synthesis was carried out[56]. The film with the counterion removed (reduced) has been measured to be about 15μm thick[69]. The thickness of the PVDF membrane is 110μm.

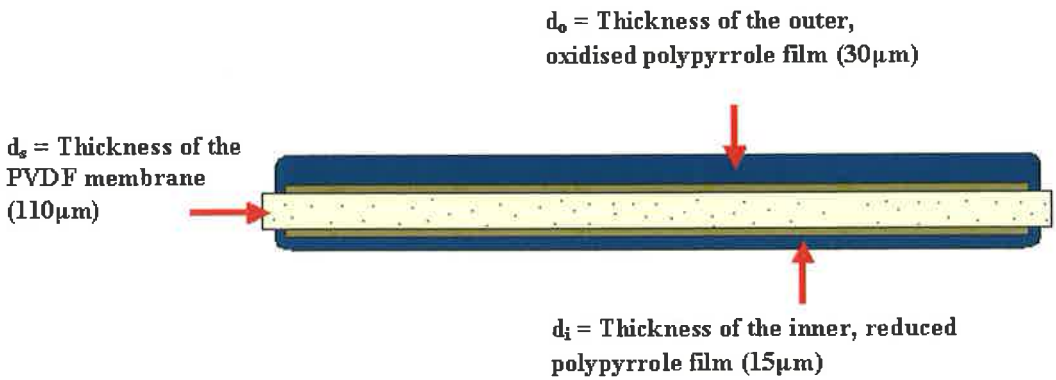

Figure 3.8: Schematic showing component thickness for the strain calculation. The d_s value corresponds to the PVDF membrane thickness, d_o to the thickness of the outer, oxidised film and d_i to that of the inner, reduced film. There is a concomitant bending of the actuator in the downward direction due to the influx of anions to the outer polymer.

The strain was calculated experimentally by taking 2-second intervals over the potential cycle and, as can be seen in Figure 3.9, the points of zero potential correspond to the points of lowest strain. Zero potential between the two strips should correspond to an equal counterion concentration in the two films, with the actuator being subsequently positioned fully upright. Likewise at a maximum potential difference between the two sides there is maximum strain according to the actuator being bent over to the greatest extent.

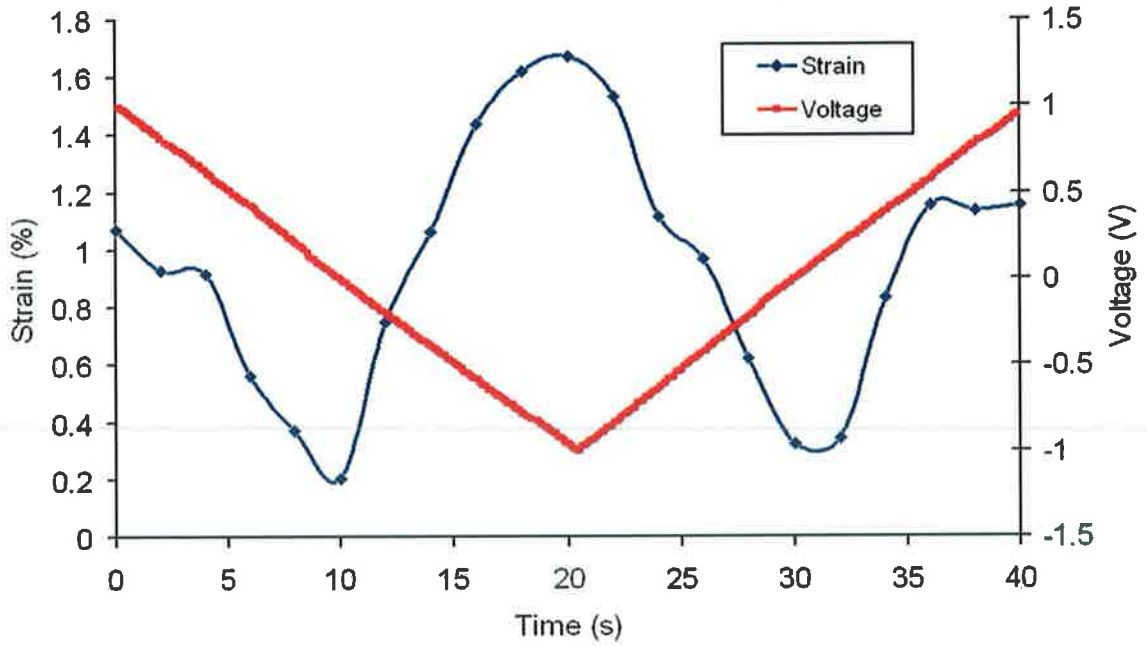

Figure 3.9: Strain response in correspondence with the voltage wavesignal.

Time (s)	θ (degrees)	θ (radians)	Radius (cm)	Strain (%)	Voltage (V)
0	109.5	1.91	2.62	1.07	0.99
2	95.0	1.66	3.02	0.93	0.79
4	93.5	1.63	3.06	0.91	0.61
6	57.5	1.00	4.98	0.56	0.41
8	38.0	0.66	7.54	0.37	0.20
10	21.0	0.37	13.64	0.21	-0.01
12	76.5	1.34	3.75	0.75	-0.20
14	109.0	1.90	2.63	1.07	-0.40
16	147.0	2.57	1.95	1.44	-0.61
18	166.0	2.90	1.73	1.62	-0.79
20	171.0	2.99	1.68	1.67	-0.97
22	157.0	2.74	1.83	1.53	-0.83
24	114.0	2.00	2.51	1.11	-0.62
26	99.0	1.73	2.89	0.97	-0.42
28	63.5	1.11	4.51	0.62	-0.21
30	33.0	0.58	8.68	0.32	0.00
32	35.0	0.61	8.19	0.34	0.20
34	85.0	1.48	3.37	0.83	0.39
36	118.0	2.06	2.43	1.15	0.58
38	116.0	2.03	2.47	1.13	0.79
40	118.0	2.06	2.43	1.15	0.97

Table 3.2: Bending angle, strain percentage and voltage at each 2-second interval of the cycle.

It can be noted that at the points of zero potential, at the 10-second and 30-second intervals the strain is at its lowest values. This corresponds with the actuator being in the vertical position, midway between the two extremes and showing similar counterion concentrations in both sides of the films. The deciding factor in the calculated strain of the film, as evident from Equation 3.2, is the radius of the circle spanned by the polymer arc, so there is an inverse relationship between it and the calculated strain. From Figure 3.6 it is clear that the more bending that has occurred, the smaller the circle spanned by the actuator will be. Thus the smaller the radius will be and the larger the strain value, as would be expected. Similarly the less strain induced on the polymer, the less bending that occurs and the larger the circle drawn will be. In a case where the actuator is completely vertical, the radius will equal infinity ($r = \infty$), and the strain will be zero.

3.3 Spectral Analysis

3.3.1 UV/Vis Spectra of the Dyes

Four acidochromic indicator dyes were used through the duration of this study; bromocresol green (BCG), bromocresol purple (BCP), m-cresol purple (mCP) and bromothymol blue (BTB). UV/Vis spectra (Perkin Elmer Lambda 900) were obtained between 350nm and 750nm for each of the dyes using solutions of millimolar concentrations. The spectra are shown below in the following four figures, showing each indicator dye made up in acidic and basic solution. The dye solutions were made up to the required concentrations, and using a pH meter (E.D.T. Instruments, RE 357, Microprocessor pH Meter) the pH values were set to acidic and basic conditions through the addition of small quantities of either 0.6M hydrochloric acid or 0.6M ammonia solutions.

Also shown below, inset within each figure, are the structural compositions of the indicator dyes in question, which are shown both in their protonated forms and in their deprotonated forms. Indicator reactions are governed by the following relation,

$$HIn + H_2O \rightleftharpoons H_3O^+ + In^-$$

where HIn represents the indicator dye in acidic form and In^- represents it in its conjugate base. The state that the indicator takes is dependant on the acid ionisation constant, or pK_a, of the dye. This represents the point at which the protonated and deprotonated states will exist in equal amounts. For the relation shown above, when the pH of an environment lies below the pK_a of the indicator dye in question the protonated form of the dye will predominate, and the equation will shift to the left-hand side. Conversely, when the pH of an environment lies above the pK_a of the indicator dye the deprotonated form will predominate. The colour of the dye changes in both of these states due to the π-bonding system associated with it. There is a change in the pattern of electron delocalisation moving from a protonated to a deprotonated state, and this results in the different colours seen either side of the pK_a value[71].

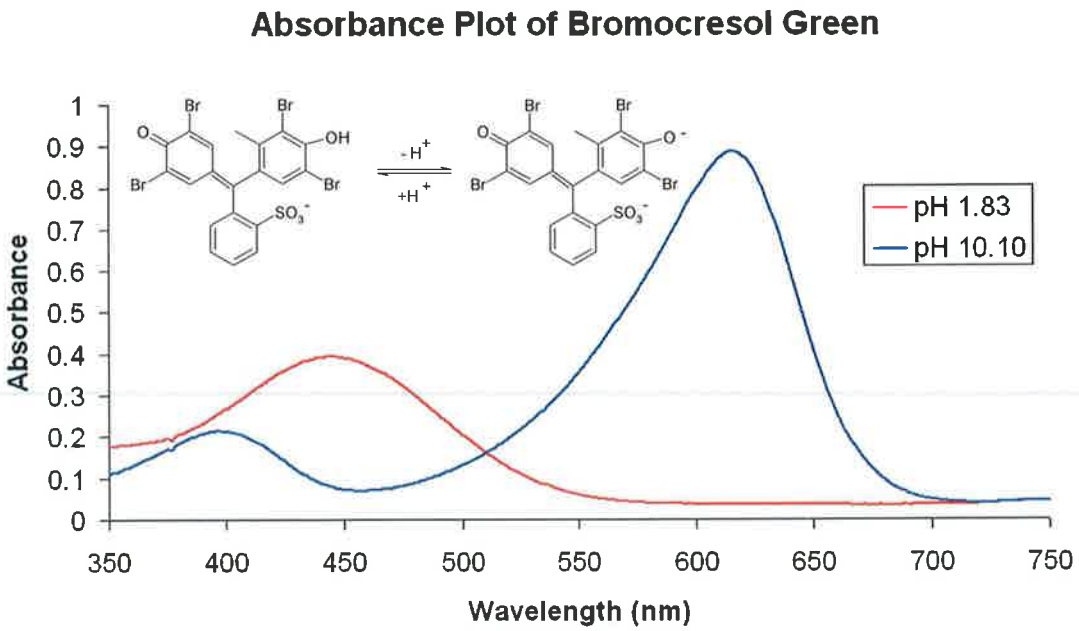

Figure 3.10: UV/Vis spectrum and structural diagrams for the bromocresol green dye. The pK_a of the BCG is 4.9[72] and deprotonation occurs through the loss of a hydrogen atom from the OH group. The charge on the SO_3^- is compensated for by association with an Na^+ cation, as the dye is available in sodium salt form[73].

As evident in Figure 3.10 the BCG dye exists in two separate forms. The acidic form of the dye predominates at pH values below pH 3.8[74], and its form is shown as the left-hand structural inset of Figure 3.10. An acid will serve as a source of protons, and in this case the acidic environment acts to donate a proton, seen in the OH functional group on the left-hand molecule. In solution above pH 5.4 the dye is converted predominantly to the conjugate base, or the deprotinated form, as the basic solution serves to accept the proton from the OH functional group to leave an O^-, shown as the right-hand structure in the inset of Figure 3.10.

The spectrum taken of the acidic (protonated) form of the dye shows a single peak at a wavelength maximum (λ_{max}) of 443nm. The colour of the dye in the pH 1.83 solution is a straw yellow, which is consistent given that this wavelength of absorption covers the blue end of the visible spectrum. The yellow region of the spectrum (570 – 590nm) shows no absorption and so is a principal component of the light transmitted through the sample or reflected back for us to see. This corresponds

to the fully protonated state that we would expect to be dominant at pH < 3.8, with no absorption evident due to the basic form of the dye.

In the basic (deprotinated) form of the dye, examined in a solution of pH 10.10, the principle peak is located at λ_{max} = 615nm of the visible spectrum. The deep blue colour of the solution is substantiated by the high absorbance value in the red-through-yellow region of the spectrum, allowing transmission only of the blue light. The dye would be expected at pH > 5.4 to show the fully deprotonated form dominant, and there is no absorption at the acidic maximum. A small peak is however evident at λ_{max} = 400nm, which corresponds to the lower violet region of the visible spectrum moving into the UV.

The acid ionisation constant, or pK_a, for the BCG is 4.9[72]. This represents an equilibrium between the protonated and deprotonated states of the dye molecules, and specifies that the two exist in similar quantities at this point. At pH values moving above this figure the concentration of the deprotinated form will become rapidly more predominant, which can be described by the sigmoid nature of the process. In the region of the pK_a value there is a large rate of change in the concentrations of the acidic and basic forms of the dye, which is represented by the steep slope of the sigmoid at this point. As the acidic and basic forms become fully dominant the slope of the plot levels off dramatically, and the rate-of change becomes minimal.

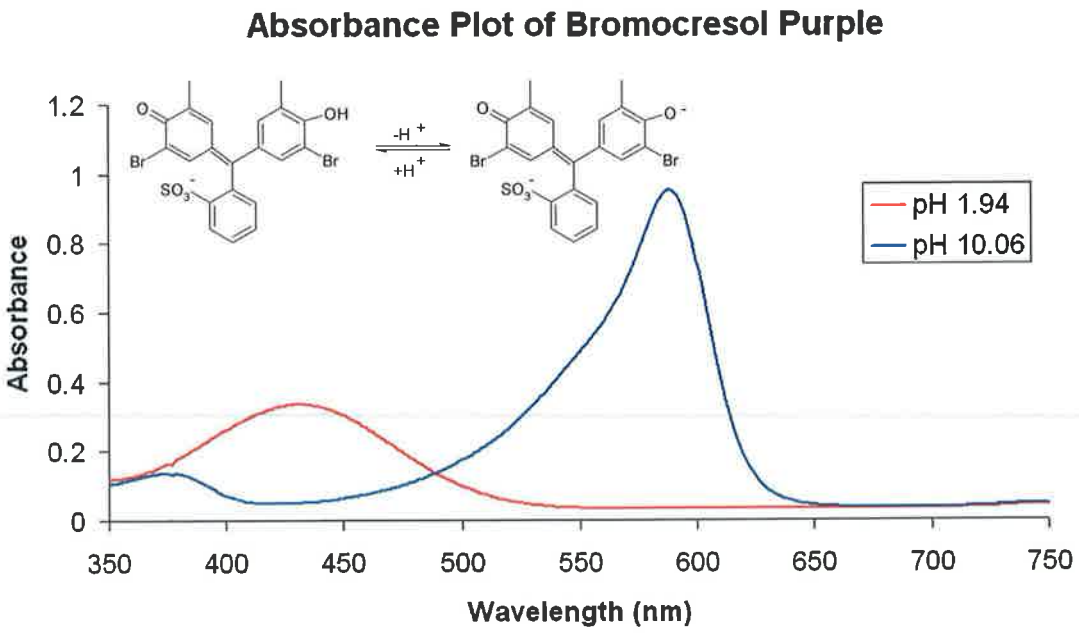

Figure 3.11: UV/Vis spectrum and structural diagram of the acidic and basic forms of bromocresol purple, the pK_a of which is 6.3[71].

The two forms of the BCP dye are shown in the spectrum of Figure 3.11, and show a distinct resemblance to that of the BCG spectrum. In acidic solution (pH = 1.94) the dye becomes protonated, resulting in a λ_{max} = 430nm. Because the protonated form of the dye predominates at pH < 5.2[74] there is again no sign of any absorption at the red end of the spectrum. This results in a pale yellow colour being displayed by the dye in solution. There is again a stronger absorbance concerning the deprotonated form of the dye (At λ_{max} = 588nm) in solution. This form predominates at pH > 6.8.

The reaction that occurs in acidic and basic conditions again gives two different forms of the dye. The protonated form occurs in the pH 1.94 solution (shown on the left-hand side of the inset equation in Figure 3.11) where the OH group is formed, while beyond the pK_a value of 6.3 the basic form predominates, whereby the proton is donated to leave an O^- on the molecule (Shown on the right-hand side). This yields two differently coloured forms, and this is what is exploited in the pH sensing methodology.

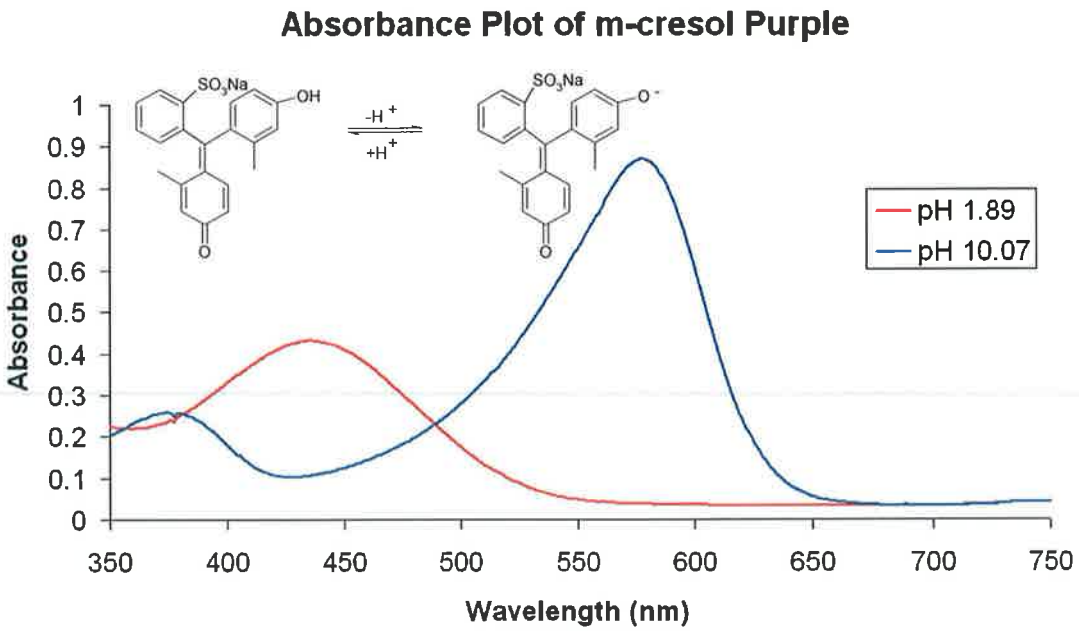

Figure 3.12: UV/Vis spectrum and structural diagram for acidic and basic forms of m-cresol purple, the pK_a of which is 8.3[75].

The spectrum for the mCP shows a colour change from a bright purple in the basic pH of 10.07 to a pale, watermelon red in acidic pH 1.89. In the deprotonated form at the pH of 10.07 the λ_{max} is 576nm, while there is very little absorption between 400 - 450nm, which is around the wavelength of purple light. There is a distinct absorption band moving below 400nm, which is stretching towards the ultraviolet region of the spectrum. In the protonated form, the dye is yellow (at pH 1.89) because the absorption maximum lies at λ_{max} = 440nm, encompassing the blue region of the spectrum, with a lack of absorption at wavelengths 550nm and greater.

The inset diagram of Figure 3.12 shows the protonated from of the dye on the left-hand side, where the proton has been included in the form of the hydrogen ion on the OH functional group. The right hand side features the deprotonated form where the hydrogen ion has been taken into the basic solution, leaving an O^- bond in its place.

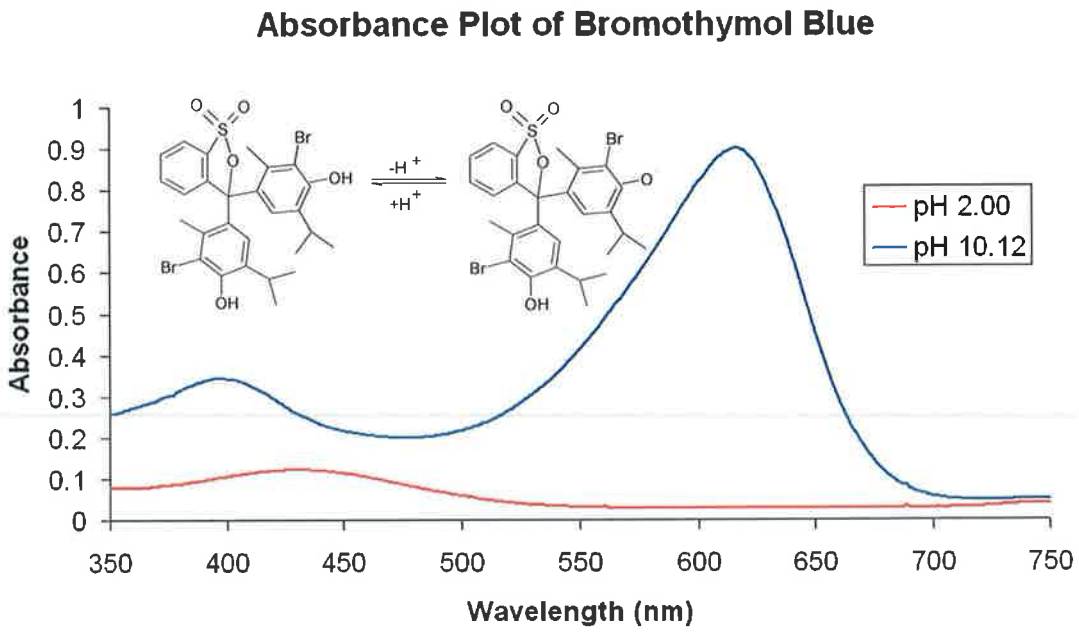

Figure 3.13: UV/Vis spectrum and structural diagram of acidic and basic forms of bromothymol blue, the pK_a of which is 7.1[76].

The protonated form of the BTB dye is a pale straw yellow colour, with a lower absorbance at the λ_{max} (here at 430nm) than for any of the previous dyes. Because of this slight absorbance the dye appears only as a very watery yellow colour, though in the case of the deprotonated form the absorbance is much greater at the λ_{max} of 615nm. The inset structural diagram shows on the left-hand side the protonated form of the dye, corresponding to the BTB in acidic solution where the hydrogen ion forms the OH group. On the right-hand side the deprotonated form is featured, with the BTB in basic solution, and an O^- group is present due to the hydrogen ion being removed. In BTB there are two OH functional groups on the molecule, though there is only one relevant pK_a value in the literature, suggesting that a second deprotonation occurs only under extraordinary conditions.

The four absorbance spectra shown above demonstrate the extent of the change between the basic and acidic forms of the dyes, and this can be used as a very useful basis when evaluating the application of polypyrrole actuators to chemical sensing, as demonstrated in Section 3.5.

3.3.2 LED Emission spectrum

The spectrum for the emitting LED in the emitter/detector setup, which will be described in the next section, is of some importance as it helps to describe the signals that are obtained from the dyes. Only the BCG and the BTB dyes were analysed using the LED configuration. The spectrum of the 627nm LED is shown in the following figure.

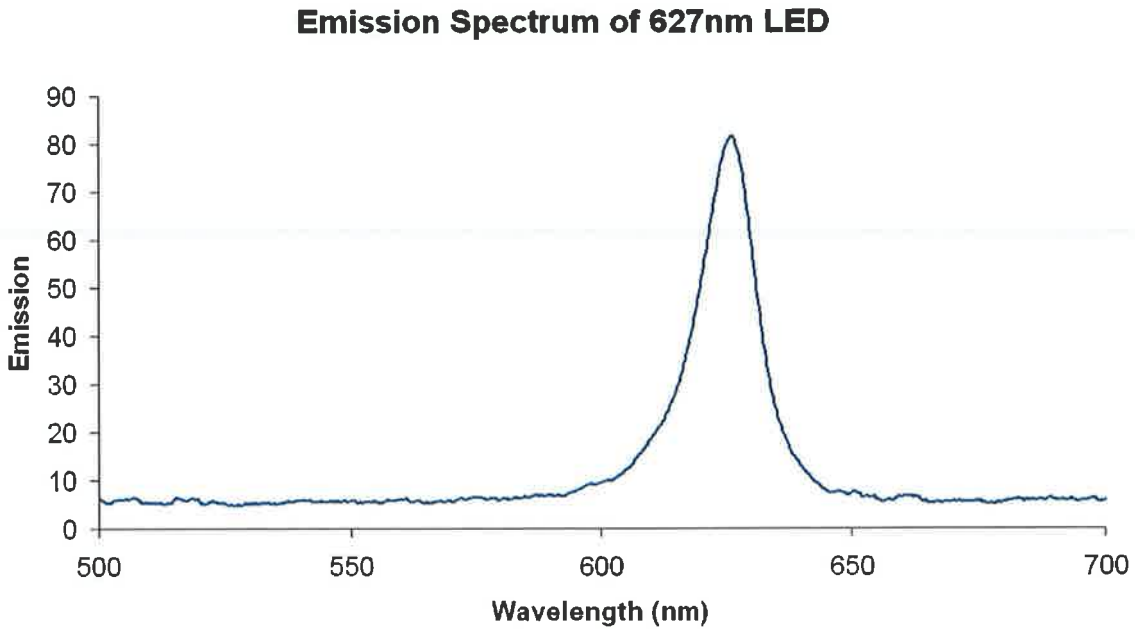

Figure 3.14: Emission spectrum of the 627nm LED.

With the emission peak being located at around 627nm there are a number of points to highlight with regard the absorption spectra of the BCG and BTB dyes. The absorption peak for the basic form of BCG (λ_{max} = 615nm) shows an excellent overlap with the emission peak of the LED shown here. This suggests that a large extent of absorption would be expected of the LED light by the basic form of BCG, with much less absorption from the acidic peak (λ_{max} = 443nm). Therefore, by monitoring the light intensity of the LED output, through a solution or film containing the dye, it should be possible to follow changes in the dye form.

3.4 LED Analysis

The LED emitter/detector system comprises two LEDs and is based on connecting the emitter diode in forward bias and the detector diode in reverse bias. A simple battery-powered microcontroller circuit controls the sensor and provides data over a standard RS-232 serial connection. The detector LED, because it is connected in revere bias does not allow the flow of a current and so acts as a capacitor, storing a 5V charge applied to the anode with respect to ground (See Figure 3.15).

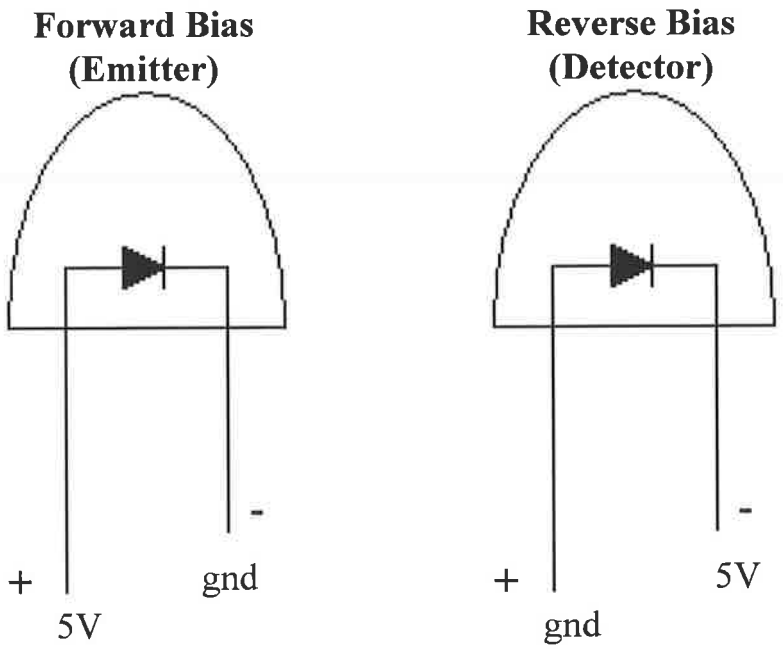

Figure 3.15: Schematic of the emitter and detector LEDs. LEDs are based on the combination of a p-type and an n-type semiconductor, in a setup known as a p-n junction. Under an externally applied potential, the diode can be connected either in forward bias or in reverse bias, as shown in the above figure. In a forward biased diode the positive and negative charge carriers (of the p and n-type materials respectively) are located near the junction, causing a current to flow between the battery terminals. In the case of a forward-biased LED photons are emitted in the process. Reversibly connecting an LED results in the charge carriers are attracted to the battery terminals, causing a separation of the charges across the junction resulting in negligible current flow. For use as a detector the reverse biased LED is charged, as

in a capacitor, and a measurement is made of the time it takes to discharge, which is based on the ambient light surroundings.

The detector LED is charged for a fixed period, typically 100μs, as shown in Figure 3.16. At this point the microcontroller switches the I/O pin used to control the detector LED from an output (+5V) to a high impedance input. This causes the voltage stored in the LED to be discharged, as can be seen in section B of Figure 3.16. The time it takes to be discharged is dependent on the light intensity of the surroundings, as incoming light causes recombination of electron-hole pairs in the LED semiconducting material, resulting in the generation of a small photocurrent (on the order of nA). The magnitude of this current is what dictates the time taken for a discharge of the 5V stored in the LED. The more light from the surroundings, the greater the photocurrent generated and the steeper the voltage discharge will be. Conversely, the darker the surroundings the longer it will take for the charge to be released from the LED's capacitance.

The sensing is based on the logic state of the input pin. The microcontroller used was operating at 20MHz and hence was capable of executing 5 million instructions per second (5MIPS). In this case the time taken to acquire each reading is 4.6μs. A fixed number of measurements were taken (14,000) resulting in a maximum sensor value of 64400μs. Over this time period 14,000 measurements are thus taken of the logic state of the input pin, which will correspond to logic 1 if the voltage is above a threshold value of 1.7V. Anything below this value will correspond to logic 0. The total number of logic 1 values is stored in a software counter on the microcontroller, and is proportional to the time taken for the discharge of the 5V signal in the LED. The measurement is proportional to the photocurrent induced by the surrounding light environment. In this particular case a 64,400μs reading will correspond to the maximum time given for discharge of the detector LED. If after this period the logic state of the I/O pin is still 1, the microcontroller returns to the maximum value. A lower value will be returned under brighter lighting conditions and indicates that the logic threshold was crossed before the maximum sensing time of 64,400μs had elapsed.

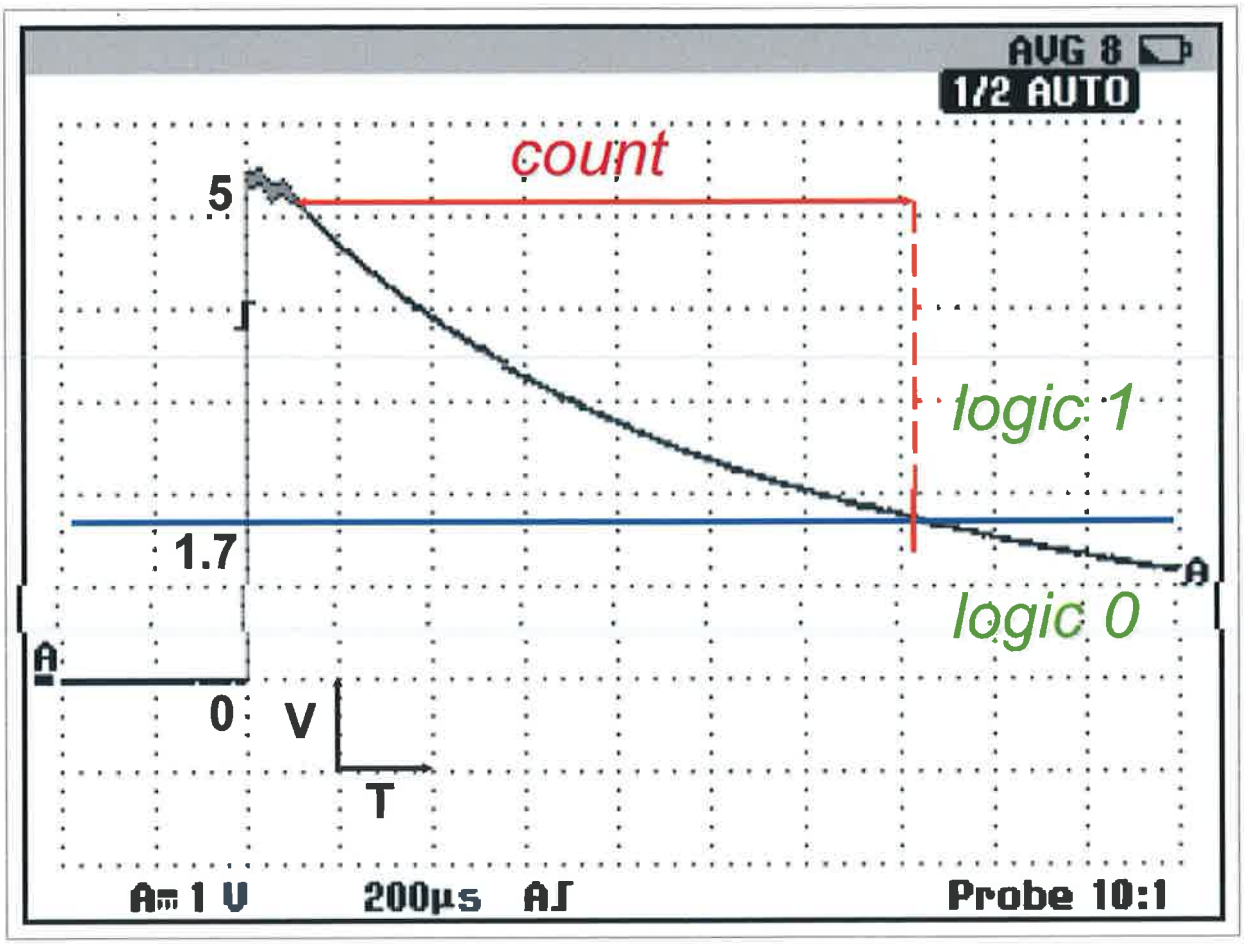

Figure 3.16: Representation of the process involved in the light-detection process of the reverse-biased LED.

The LED analysis highlights one approach for sensor detection developed using the polypyrrole actuator as a medium for sensor delivery. In the following configuration the sensor is a cresol-based dye sensitive to changes in the pH of its environment. Ammonia was used as a calibrant solution to set the dye back to a deprotonated state before it was again brought into the acetic acidic environment. This process was repeated over 110 cycles, corresponding to a two-hour period, and the response was measured over this time.

3.4.1 Response to Acetic Acid

The first experiments were run using BCG. The dye was visibly changing to a bright yellow protonated form in the acidic gas phase environment, compared to the blue-green neutral form in air. The other point to note was the rapid change of the dye once it had been added or removed from the acidic environment. To translate this visible response into a physical measurement, capable of accurately and reproducibly identifying the colours, a technique was employed that involved a colorimetric approach whereby the colour was detected through the transmission of a light source through the dye and into a detector. The dye was coated to a polyethylene substrate, and a polypyrrole actuator was used as the means of sensor delivery. The beauty of the approach was that the measurement system could now be placed in a single location with the sensor itself being moved in and out of the sensing environment. This is displayed in the following experiments where the colorimetric detector is located first within the sensing environment and secondly outside of it. In both of these cases the response of the dye is critical, particularly when measurement occurs outside of the environment and any colour-change must be long-lived enough for an accurate signal. Figure 3.17 shows the range over which the BCG dye changes between the basic form (ammonia saturated gas phase) and acidic form (acetic acid saturated gas phase). Figure 3.18 shows a schematic of the sensor setup that was used in the experiment.

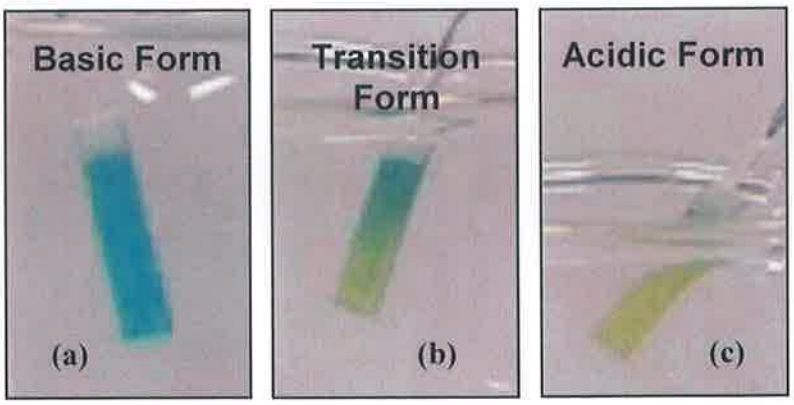

Figure 3.17: Photos of the BCG-based sensor in (a) ammonia environment, (b) being introduced into the acetic acid environment and (c) steady-state colour in the acetic acid environment.

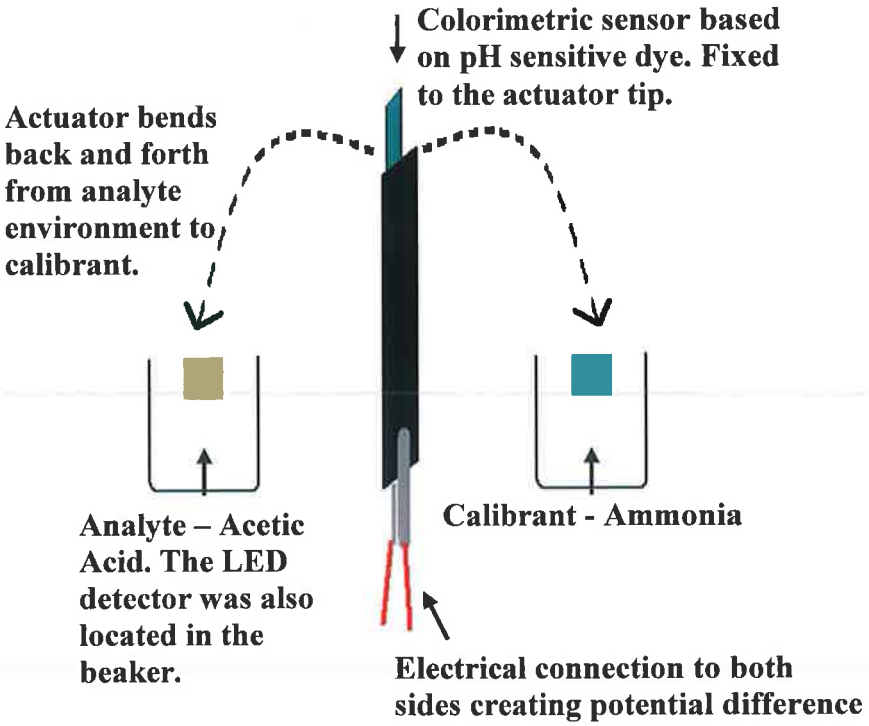

Figure 3.18: Schematic showing the system set up to colorimetrically monitor the response of the dye when moved into an acidic environment. The LED detector system was located in the acetic acid to monitor the response. Ammonia was used as the calibrant material to change the dye back to the blue deprotonated state.

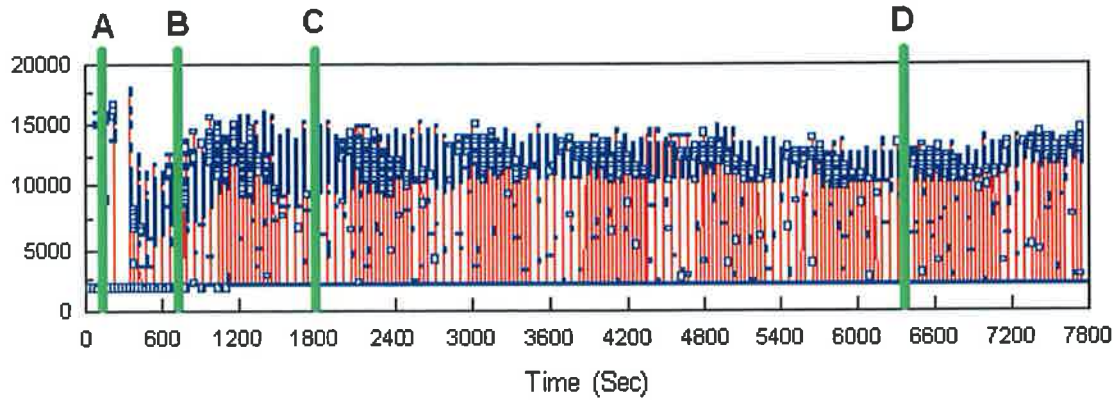

Figure 3.19: A complete plot of the colorimetric response of the system over 2 hours. The response is shown by the blue data points, which increase as the sensor is brought in between the two LEDs by the polypyrrole actuator. The LEDs were glued to the inside of a glass beaker, which served to provide the environment for analysis. Approximately 110 cycles were covered during the experiment's duration, and the labels A, B, C and D represent points in the experiment which will be discussed later in the text.

The data shown in Figure 3.19 gives a full overview of the response that was generated over a two-hour analysis period. The lower line in the plot shows the baseline signal where there is a saturation effect due to the intensity of light entering the system from ambient lab conditions. When the sensor is brought between the emitter and detector LEDs there is an increase in the signal due to the decrease in light intensity. This is due to the light being transmitted through the sensing substrate and is thus representative of the colour, and hence the protonation state, of the dye. In this experiment the beaker in which the LEDs were located was left empty for the first number of cycles before the acetic acid was added. This acted as a control for the subsequent results of the sensor response in later cycles. Essentially it was hoped that the technique applied would be able to demonstrate the potential of the actuator system for the reproducible delivery of a sensing medium to a detector. The following results in figures 3.20 through 3.23 are shown for the response at different stages of the experiment, labelled A, B, C and D in Figure 3.19 above.

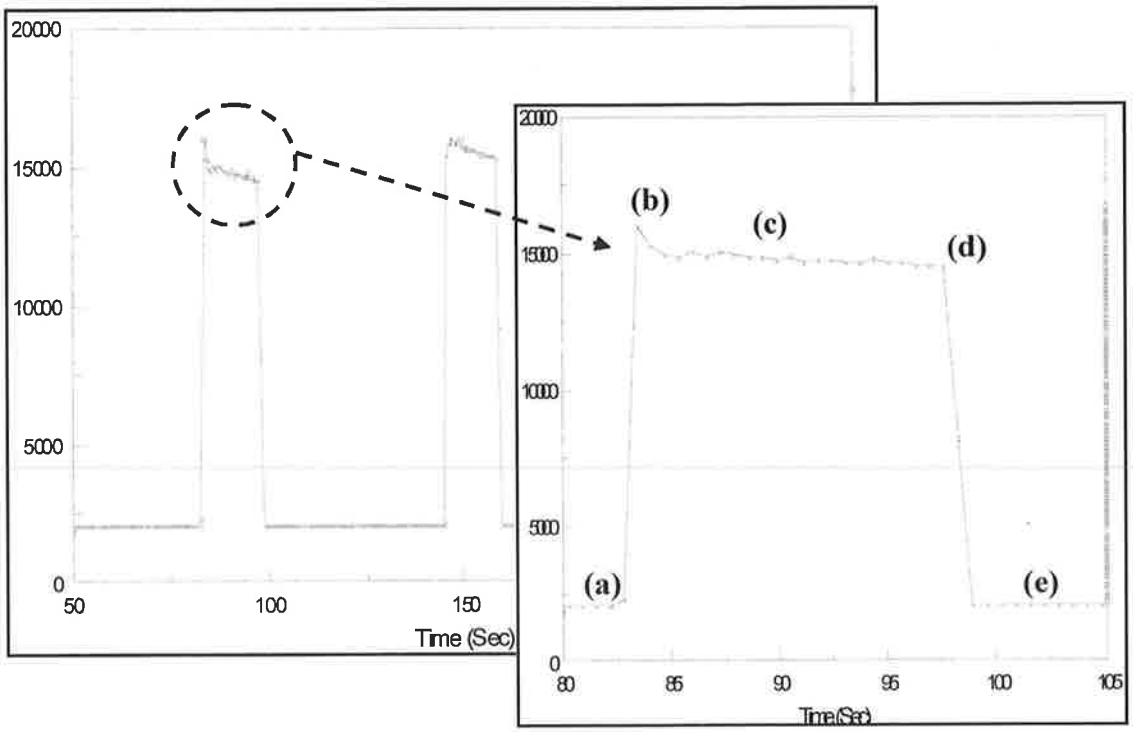

Figure 3.20: Cycle 1: A plot showing the response from the sensor after 83 seconds has elapsed in Figure 3.19 (Labelled Point A). At this point no acetic acid had yet been added to the system.
(a) refers to the baseline signal, which is detected before the sensor is brought in between the LEDs by the actuator at (b). The time that the sensor remains in between the two LEDs is indicated by (c), before it is brought out again by the actuator at (d). The sensor response then returns to the baseline region at (e).

The first point of note from Figure 3.19 comes after 83 seconds. The data here has been taken before the acetic acid has been introduced. As can be seen from Figure 3.20 the response generated is a relatively flat one. Although there is an initial peak as the sensor is moved in, the signal quickly becomes steady and remains essentially static at around 15000 on the y-axis. The difference between the signal at the initial peak (At (b) in Figure 3.20) and the signal as the sensor is removed from the detector (At (d) in Figure 3.20) is signified by ΔS, which in this case is 1471. A summary of the ΔS values for each plot can be found in Table 3.3. The change in the detector signal upon introduction of the sensor represents the colour of the sensor in basic form (blue), which is used as a calibrant to maintain the dye at an initial colour when introduced to the detector. There is little change in the colour in the empty beaker, as

is indicated by the flat response. For subsequent readings of the data it is expected that the sensor should begin at this value before the response of the dye to the acid lowers the intensity reading, as the dye turns yellow and more light from the emitter LED is transmitted due to a decrease in the absorbance at wavelength $\lambda = 615$nm. The rate of response of the dye can also be measured by the extent at which the signal is changing over time.

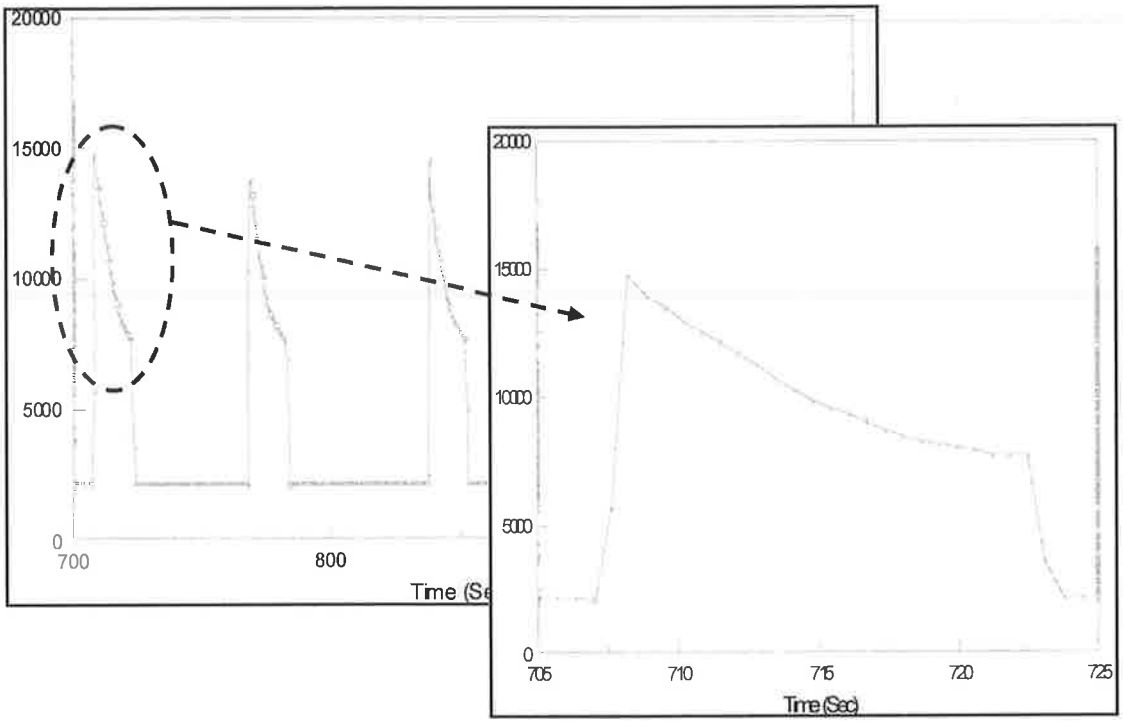

Figure 3.21: Cycle 10: Plot showing the response from the sensor after 707s (Point B) in Figure 3.19. Acetic acid has now been added to the beaker.

Upon the addition of the acetic acid there is a change in the response of the sensor. As can be seen from Figure 3.21 the initial response is again at 15000, as previously for the stage involving no acid, but because the dye is now responding to the acetic acid environment, the changing colour prompts a decrease in the signal as more light is allowed through to the detector. The initial blue colour of the sensor represents the basic, deprotonated form of the dye, which absorbs strongly in the 600-630nm region of the visible spectrum (See Figure 3.10). Because the LED emits at 627nm (Figure 3.14) there is a large absorption of this emitted light and hence little transmission. As the sensor is introduced to the acetic acid environment the dye

changes to a protonated, yellow form, which according to Figure 3.10 absorbs very weakly in the 600-630nm region. For this reason more light is transmitted and the signal decreases as the state of the dye changes from deprotonated to protonated, as seen in Figure 3.21.

The rate of the response is rapid over the 20-second measurement as there is a $\Delta S = 7097$. There is however a tailing off of the signal towards the end as the dye approaches a steady-state value.

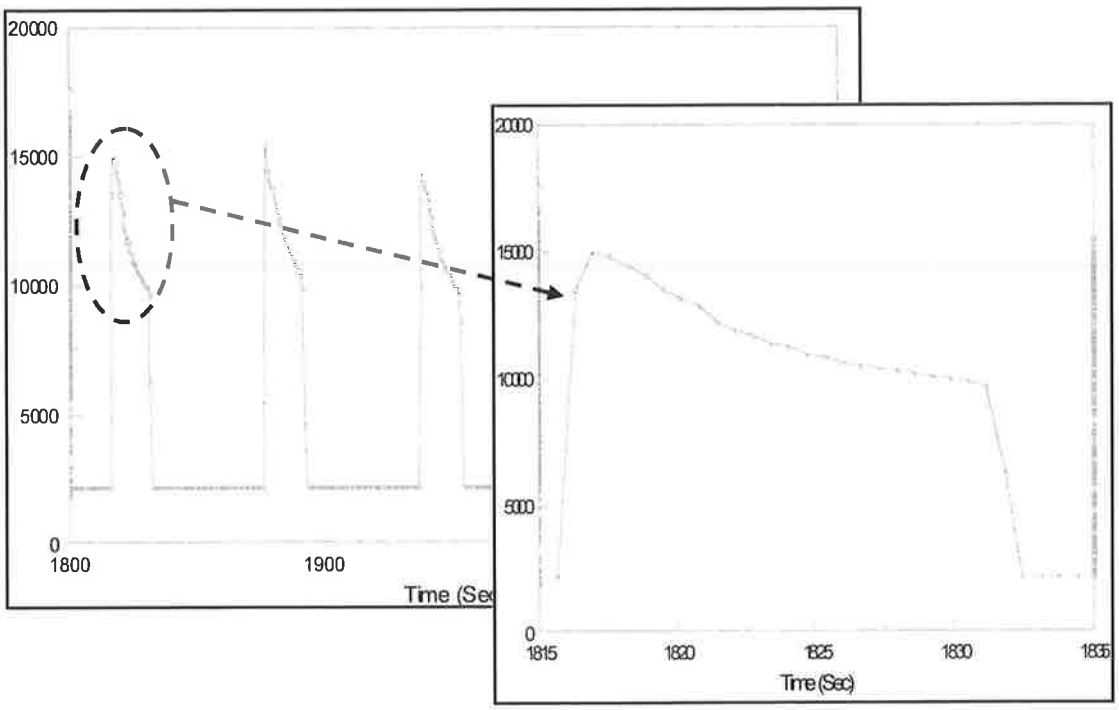

Figure 3.22: Cycle 25: Plot showing the response of the sensor after 1815 seconds (Point C in Figure 3.19).

Figure 3.22 shows a progression of the response after the initial addition of the acetic acid. Now that the system has been running for just over the 1800 second-mark a comparison to the previous figure reveals visually that there is a clear decrease in the change in signal from when the sensor was introduced to the system to when it was removed. By the time the 20-second measurement has been completed $\Delta S = 5323$, and with the basic signal still up at the 15,000 mark there is an indication that the protonated state of the BCG is no longer as prominent, or that it now requires more time to reach a steady state. In the latter case there may have been a decrease in

the rate of response of the dye, indicating a degradation effect possibly attributed to repeated exposure to concentrated acetic acid fumes and constant switching of the protonation state. Another possibility in the signal degradation is that the LEDs themselves have become coated with the acidic fumes, though this would be expected to affect both the basic and acidic signals.

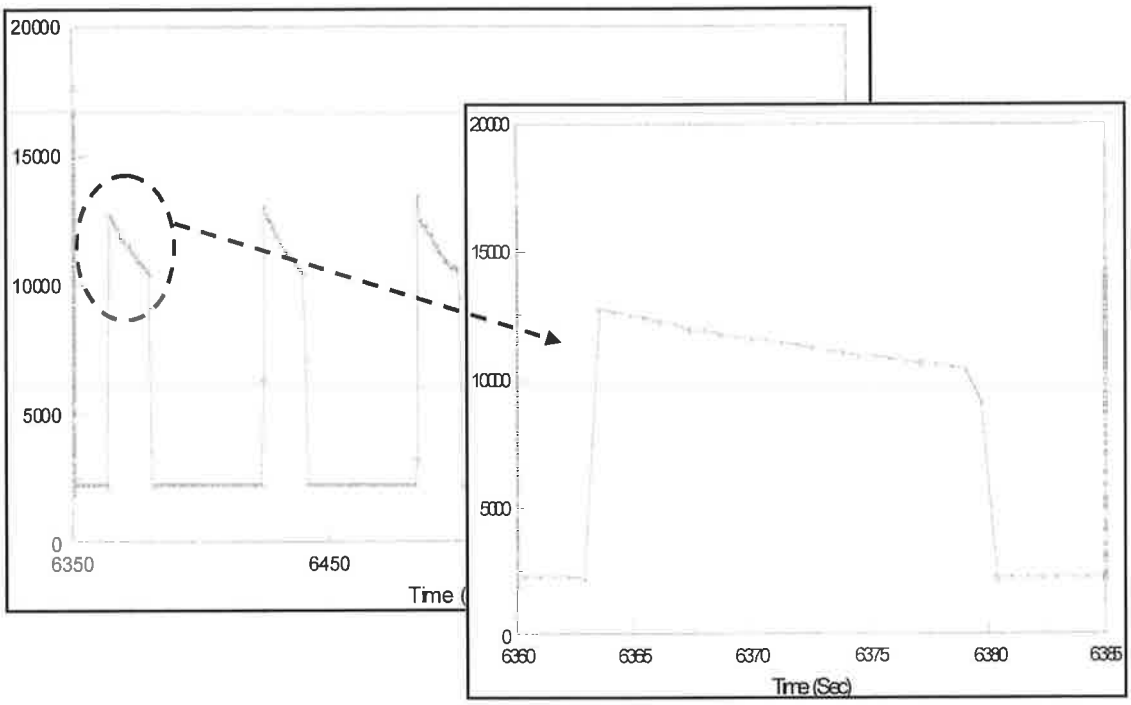

Figure 3.23: Cycle 90: Plot showing the response of the sensor after 6360 seconds (Point D in Figure 3.19). This data was taken on approaching the end of the experimental run.

As can be clearly seen in Figure 3.23 above the signal has now decreased on both counts regarding the protonated and deprotonated states, giving a much flatter response than initially encountered. The extent of colour change in and out of the acidic environment has narrowed considerably with the change in signal $\Delta S = 2421$, compared with 7097 upon initial introduction of the acetic acid. The results are summarised in Table 3.3. One method to perhaps improve interpretation of this data is an increased exposure time to the volatile acid. This would help to allow the response to reach a full steady-state value, and would perhaps result in less of a fall in the ΔS value. Consequently though, the results suggest that an increasing amount of time

would be required to reach steady-state as the number of cycles increase. In the earlier responses, as in Figure 3.21, there is a suggestion that the steady state has been reached due to a tail-off of the signal towards the end of the cycle. Thus the rate of change in the dye is also seen to decrease over time, as the protonation effects in the acidic environment occur at a slower rate towards the end of the experiment. The following table summarises the effects noted.

Cycle	Detector Signal (Basic form)	Detector Signal (Acidic Form)	ΔS
1 (Control)	16029	14559*	1470
10	14758	7661	7097
25	15000	9677	5323
90	12734	10313	2421

Table 3.3: Figures showing the detector responses for the basic and acidic forms of the BCG, and also the difference in signal between the two values (ΔS).

*This value does not correspond to the acidic form because the acetic acid had yet to be added, the value relates just to the signal as the sensor left the detector.

As can be seen from Table 3.3, there is a decrease in the ΔS value over time as the experiment progresses, while the extent of the signal for the basic and acidic forms of the dye is seen to decrease by the 90th cycle. The experiment does, however, show that the technique works, especially with respect to the polypyrrole actuator-based delivery mechanism. A sensing device capable of self-calibration has thus been demonstrated, with the actuator forming the basis of delivery for a sensor from a sensing environment to a calibrating one.

3.4.2 Response Across a Range of pH Values

One issue surrounding the use of the LED setup was the reproducible locating of the sensor directly between the LEDs. Ideally the LEDs are positioned as close together as possible, to eliminate any ambient interference. However, with regards to the sensor, which is fixed to the end of the actuator, it becomes more difficult for it to be placed in between the LEDs the closer they are together. This is due to an uncertainty in the precise positioning of the sensor at each vertice of the cycle. It is important also to keep the sensor surface as perpendicular as possible to the light from the emitter LED, or at least to keep this incident angle reproducible between cycles. As the angle changes, so to does the path length of the incident light through the sensing substrate, a property that could influence poor reproducibility of results. In order to tackle these problems, a structure was designed with a view to eliminate the discrepancy in sensor position, as shown in the schematic of Figure 3.24.

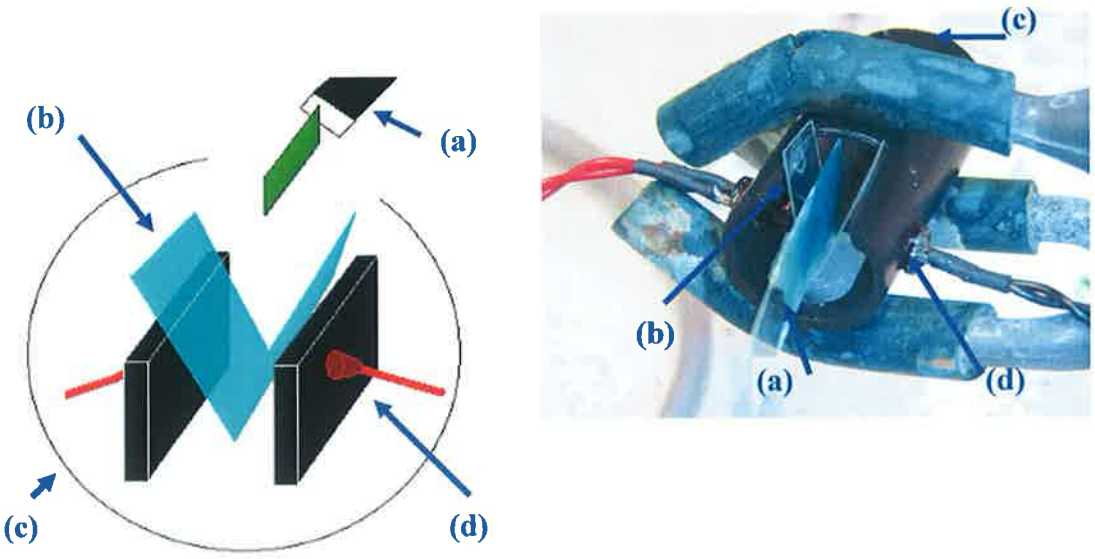

Figure 3.24: A schematic of the LED setup is shown in the left-hand diagram, with the sensor entering the setup (a). The model is composed of a V-shaped piece of transparent PET (b), glued to the base of a cylindrical housing (c) in which two LEDs were embedded facing opposite to each other (d). The housing acted as a partial shield to ambient light, as well as a platform to support the guide. The LEDs were both coated in black dye around the edges, leaving only a small exposed window at the very tip, so as to further enhance this signal. The photo on the right-hand side shows the actual device (with a sensing tip inserted to the guide) used in the measurements.

The LED setup was put into practice through a colour detection experiment, conducted across a range of pH solutions; the schematic is shown in Figure 3.25. Two separate experiments were run, the first involving a manual technique to test the efficiency of the dye with the LED setup and the second implementing the polypyrrole actuator to deliver the sensor to the LEDs. Comparison between the two techniques was primarily based upon the reproducibility of the signals and on the ability of the data to identify the pK_a of the dye in question. The dye used on this occasion was bromothymol blue (BTB), which exhibited a colour change that lasted beyond removal from the solution, and the substrate for the sensor was PET. The pH solutions were generated using pH buffer tablets (pH 4.0, pH 7.0 and pH 9.2, Fluka), a sodium hydroxide (NaOH) solution to vary the pH and a pH meter (E.D.T. Instruments, RE 357, Microprocessor pH Meter) to measure the solutions before the test, and the range was set from 5.5 to 9 in 0.5 increments.

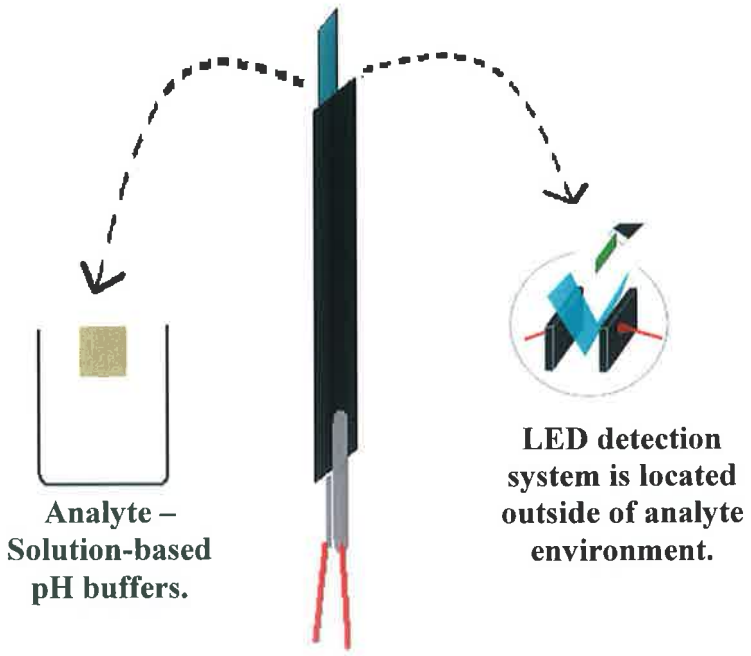

Figure 3.25: Schematic for the setup for analysis of the response of bromothymol blue across a range of pH values.

The dyed substrate gave an opaque effect due to being supplemented with titanium dioxide (TiO_2), and although the material was found to degenerate over time the experiments were carried out under a short-enough time-frame that no perceivable degradation, in the form of fading colour, was evident. The solutions were in this case immersed in each pH solution for ten minutes before they were exposed to the LED detector system, either manually or by actuator.

A solution-based approach was taken for this experiment because it proved the most efficient method of inducing a lasting colour change in the dye. It was also the most accommodating means of introducing a range of set pH values, which was important in collecting the data necessary for pK_a analysis. Five measurements were taken of each phase of the dye, each measurement lasting two minutes. The results, as discussed on the following page, indicated no fall-off of the detector signal due to the dye reverting to a neutral state.

Following the manual phase of the experiment, the next stage was to introduce the actuator to the setup. A similar experimental was followed where the sensor was again allowed to settle in pH solution and, following a ten-minute submersion period, it was removed and the actuation process was initiated. The measurements were carried out over five cyclic voltammetry cycles, whereby the dye was brought in and out of the LED detection unit. The results were slightly less uniform than were those seen in the outcome of the manual method, which was due to a greater variance in the positioning of the substrate when it was placed between the emitter/detector LEDs.

The following figures show the results obtained using the manual approach (Figures 3.26, 3.27) compared to the automated measurements (Figures 3.28, 3.29).

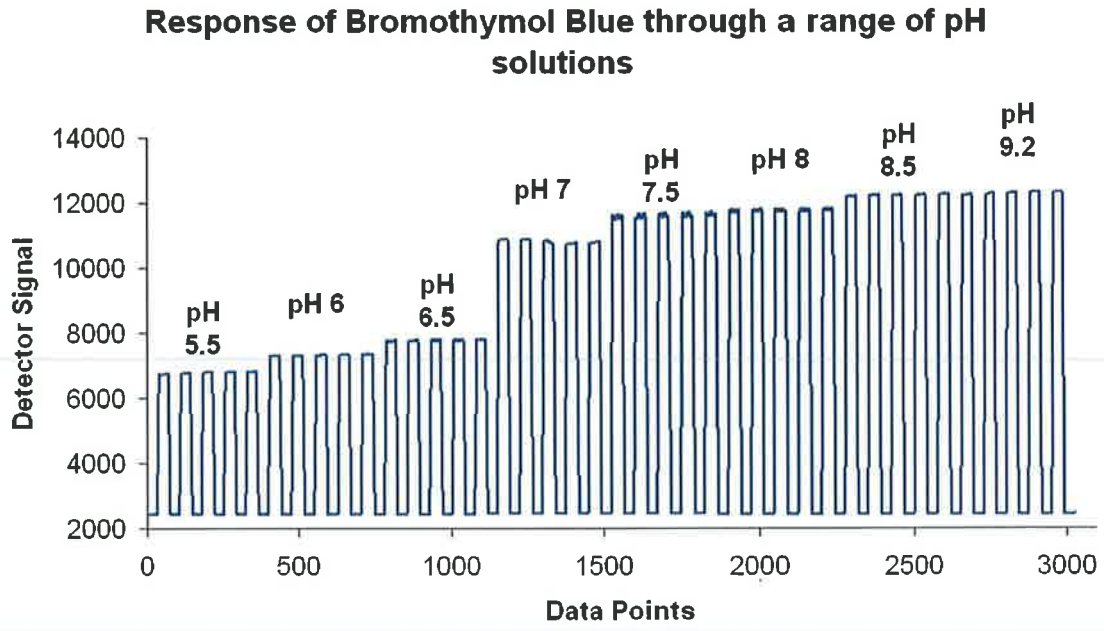

Figure 3.26: The figure shown represents five runs of the sensor conducted at each pH value, with the detector signal increasing as the BTB changes from a protonated to a deprotonated state. These values were taken to form five pK_a calculations, which were then averaged. The BTB sensors were inserted manually to the detector.

The first experiment was conducted manually. The dye was coated onto the PET substrate and then immersed in the pH solution for a period of ten minutes. The sensor was then placed into the guide between the LEDs for 5 separate 2-minute measurements. The results for the procedure can be seen in Figure 3.26 where a reproducible response is evident, coupled with a quite definite delineation between pH values. The figure uses a seven-point moving average filter to generate a less noisy signal, which, when the sensor was present, tended to fluctuate a small bit, though this was not largely significant compared to the extent of the signal. From this data a separate plot was generated to chart the average intensity against the increasing pH increments, which resulted in a sigmoid. From this a second derivative plot was created to chart the data as a function of the change in detector signal. The point of greatest change refers to the acid ionisation constant or pK_a, the point beyond which the dye becomes protonated or deprotonated. Figure 3.27 displays this information.

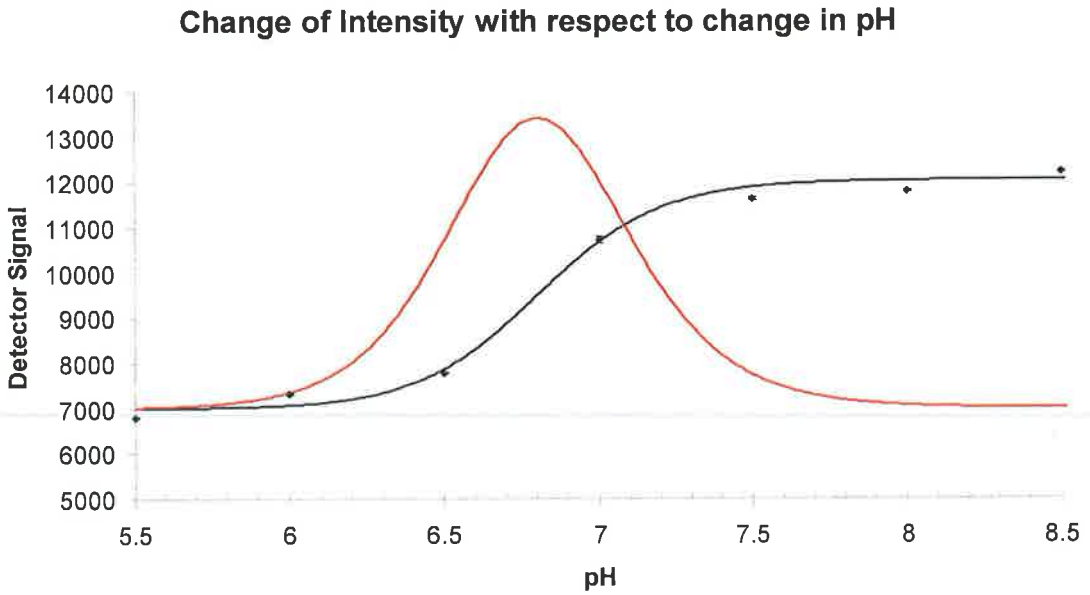

Figure 3.27: A run of the experimental data points and best-fit sigmoid model that form the basis for the pK_a determination in the BTB dye. The change in the detector signal across the range of pH values 5.5 – 9.2 is shown by the black data points in the above diagram, with the black line denoting a best-fit approximation. The red line displays the first derivative data of the experiment, which describes the greatest rate of change in the pH, corresponding to the pK_a (BTB = 7.1[76]) of the dye. Experimental points are averages as shown in Table 3.4 (n=20). The standard deviation is plotted as error bars but the values are small and are hidden by the point symbols.

Figure 3.27 shows a sigmoid plot that was generated from a best-fit equation based on the experimentally acquired detector values at various pH levels. The points in Figure 3.27 are an average of values of the detector signal received from experimental measurements at the given pH values. Five runs were made of the experiment, yielding five sets of data for each pH value. A number of data figures were received for each measurement of the transmitted light at the detector so an average of twenty of the received data figures was taken. These figures were then taken as the basis for the plotting of a sigmoid curve, which was modelled according to Eqn. 3.4. This data could then be used to form an approximation of the pK_a of the BTB, which was expected to be 7.1. The data is tabulated in Table 3.4 with the pK_a values obtained for each run, along with the average and standard deviation of these pK_a calculations.

The best fit approximation was based on a similar model developed for the prediction of the response of an ion-selective electrode[77]. The formula and the parameters used are shown in Eqn. 3.4.

$$y = \left[\frac{a}{(1+\exp[b(x-c)]^{e})}\right] + d \qquad \text{(Eqn. 3.4)}$$

Where a = peak height, in this case denoted by the maximum pH value

b = slope coefficient

c = pH value at which the inflection point occurs

d = baseline offset

e = symmetry parameter for the sigmoid

y = detector signal at the point x

x = pH of the solution

The peak height denotes the maximum height that the sigmoid plot will have, and here this is denoted close to the detector value at the highest pH value. The inflection point of the sigmoid plot is the point at which a tangent can be drawn, in this case at the central region where the slope is high. The baseline offset allows the signal to begin at the detector value for the lowest pH solution.

The best fit curve was generated from the residuals of the experimental data and the predicted data. The residuals were squared and then added together (Sum of squared residuals, SSR) across the values measured. For a curve to best fit these points the sum of the squared residuals needs to be kept to a minimum. This can be achieved by applying the *Solver* function in Microsoft Excel, which will modify the variables so as to minimise the SSR count. The variables can also be modified manually to minimise the SSR count, and this can sometimes lead to a better fit of the curve visually.

pH	Detector Signal				
	Run 1	Run 2	Run 3	Run 4	Run 5
5.5	6742.35	6773.50	6801.00	6808.95	6822.75
6.0	7308.70	7316.80	7325.85	7335.65	7341.70
6.5	7752.90	7772.25	7779.00	7789.50	7790.85
7.0	10882.35	10878.55	10823.80	10738.25	10782.50
7.5	11561.95	11577.75	11633.10	11635.35	11659.65
8.0	11749.05	11757.53	11764.95	11794.95	11784.90
8.5	12196.30	12213.95	12219.45	12231.30	12245.75
9.2	12215.70	12262.05	12284.90	12303.60	12313.25
pK_a	6.80	6.79	6.80	6.81	6.80

Table 3.4: Average intensities from the pH 5.5 – 9.2 solutions for the five runs conducted of the experiment. The pK_a values obtained yield an average of 6.80 ± 0.01.

The first derivative plot was derived from the change in the intensity versus the change in pH, i.e. $\Delta I/\Delta pH$. The data was generated from the best-fit curve used in Figure 3.27, and a baseline of 7000 was used to bring the two plots onto the same scale. It can be seen from the peak of this second derivative plot that the predicted pK_a value lies at pH 6.81 in this instance, with the average pK_a across the five runs being 6.80 ± 0.01, which is a little off the expected value of 7.1[76]. This could be due to factors such as slight changes in the pH solutions after preparation, or inaccuracies in the experimental.

A second experiment was undertaken involving the use of the polypyrrole actuator to deliver the sensor to the LEDs. The sensor tip, while attached to the actuator was allowed the same 10-minute resting period in each of a new set of pH solutions before being actuated by a ±1V applied CV pulse. Five cycles were completed for each sample although adequate signals were not achieved on each measurement due to less certainty in the positioning of the sensor when attached to the actuator. This was despite the presence of the PET-fabricated guide to bring the sensor between the LEDs; hence there is a separate n-value for each pH measurement in the plot.

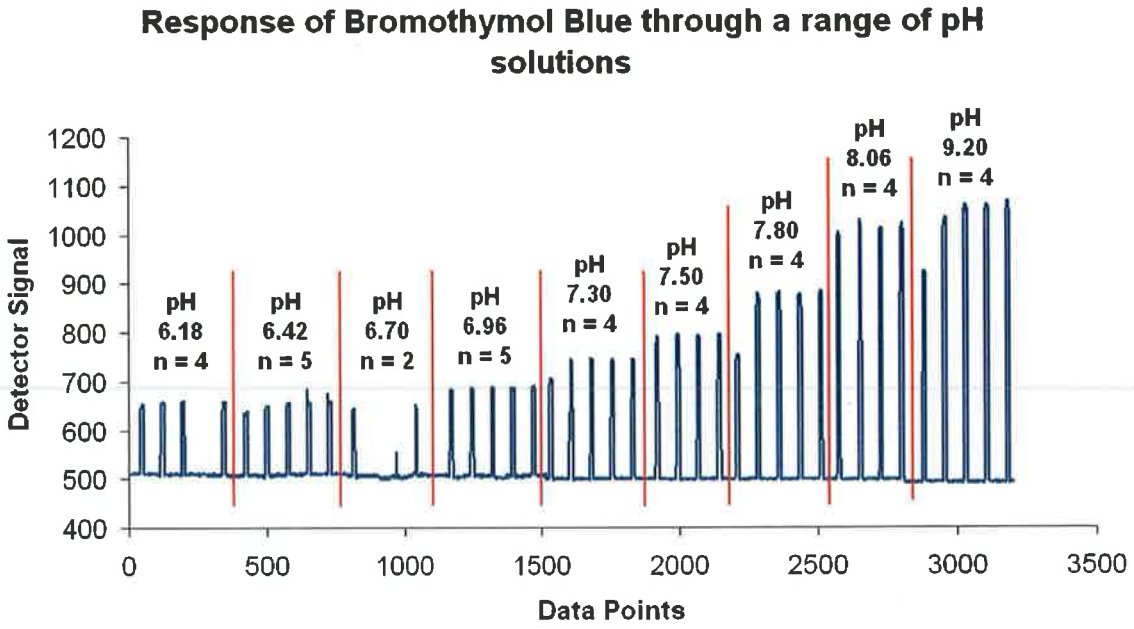

Figure 3.28: The change in intensity across a range of pH solutions. The polypyrrole actuator was used to deliver the BTB-based sensor to the colorimetric detector.

In Figure 3.28 the experimental values for the intensity changes are charted, using the polypyrrole actuator as the means for sensor delivery. While the results are distinctly more erratic than those received during the manual experiment shown in Figure 3.26 there is still a general trend though acidic to basic pHs. While this was to be expected, given that the same dye was used as per the manual method discussed earlier, the relevance lies in the technique employed to achieve the data. The data response shows the viability in the electromechanical actuator, operating at a low voltage, to move a sensor from an environment to a detector. It is evident from the respective graphs (Fig. 3.27 and Fig. 3.29) that there is a difference in the reproducibility of the data of the manual and actuator-based methods. While each of the five measurements generated a detector response in the manual method, this was not the case for the actuator. In the interests of keeping the analysis consistent the received values were used in a similar format, with a best-fit curve being drawn through experimental data (Fig. 3.29). In this instance there were gaps in the data, as can be seen in Table 3.5. In the extrapolation of the data values only those values that corresponded to each other within a pH range were used in the analysis, for example in the pH 7.30 and 7.80 in Figure 3.28 only four of the five peaks

were seen to constitute a reliable signal. Other data values did not show high levels of reproducibility because of the issue of misplacement of the sensor by the actuator, as is evident from the values for pH 6.70.

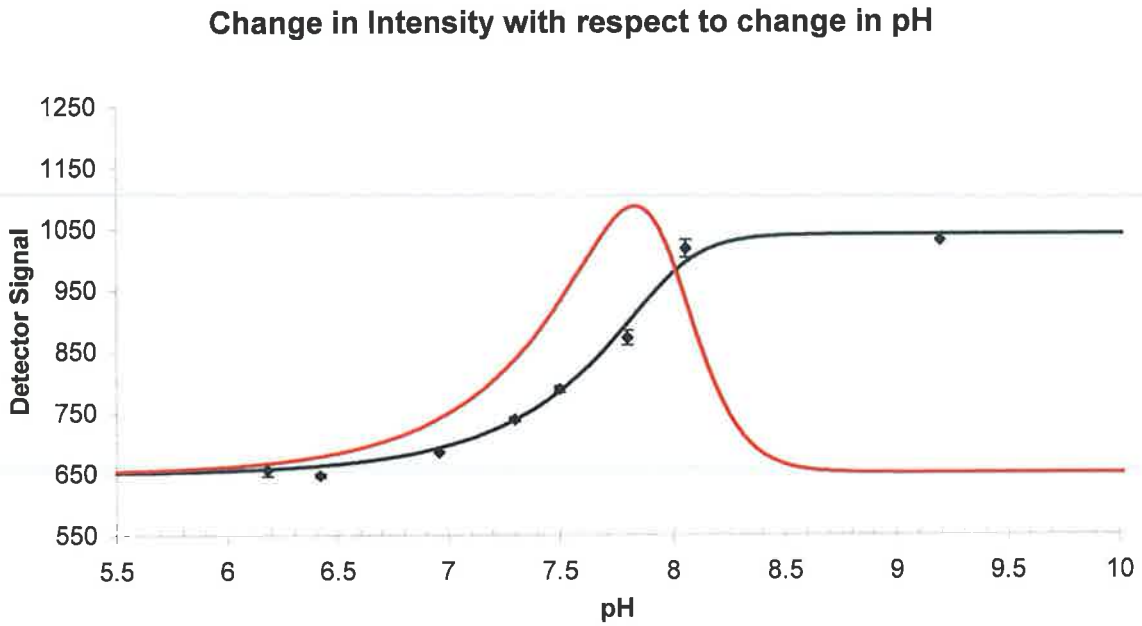

Figure 3.29: Plot showing the change in the detector signal with respect to pH. The black line indicates the best-fit line drawn around the points generated from experimental values. The red curve represents the change in intensity with respect to the change in pH, where the greatest rate of change is seen to occur at ~7.8. The baseline of this curve has again been raised to 650 for the purpose of the graph.

From the data collected a plot was again modelled from Eqn. 3.4, with the detector response to the light propagated through the BTB sensor at different pHs. From Table 3.5 below it can be seen that none of the five runs yielded a full set of data values, which would suggest that the best-fit sigmoid plot would be less accurate as a result. This is further suggested by the larger standard deviation associated with the mean pK_a calculated for this method when compared with the manual technique. The result here gives a pK_a value of 7.81 ± 0.05, which is higher than the expected value of 7.1.

pH	Detector Signal				
	Run 1	Run 2	Run 3	Run 4	Run 5
6.18	647.75	656.26	659.62	-	658.17
6.42	634.43	646.89	652.88	658.63	659.62
6.70	641.90	-	-	-	646.00
6.96	681.93	684.43	684.43	684.16	686.64
7.30	-	738.32	740.31	738.12	733.02
7.50	781.62	788.02	784.51	789.91	-
7.80	-	871.60	875.13	867.93	878.17
8.06	992.35	1017.09	1005.52	1008.40	-
9.20	-	1029.86	1054.49	1054.75	1061.71
pK_a	7.79	7.77	7.77	7.86	7.87

Table 3.5: Average intensities from the pH 6.18 – 9.20 solutions for the five runs conducted of the experiment. The pK_a values obtained yield an average of 7.81 ± 0.05.

The experiment has shown a semi-quantitative approach to pH sensing, using a low-power actuator in an automated approach. The most important thing to note is that the experiment describes a working system involving the use of a polypyrrole actuator to measure such environmental properties as pH. The greater scope of the work would be in the implementation of the design in a form of sensor capable of self-calibration, whereby the actuator serves as a means of delivering the sensor back and forth between a calibrant environment and a measurement environment. The use of the pH indicator is only an example; the technique could be applied to a range of different sensing materials, for example humidity or CO_2, and could prove important in the role of automated sensing.

A further step in the development of the technique described above would be to try to introduce it to gas phase sensing, either relating to pH or to identification and quantification of a gas species. Autonomous measurement in the liquid phase poses a number of problems, particularly concerning solution droplets becoming fixed to the surface of the sensor, which can then cause problems through being transferred onto the PET guide between the emitter/detector LEDs, resulting in subsequent pH readings being contaminated. The mechanical strength required for the actuator to remove the sensing substrate from solution is also an issue, as more power is required to break the surface tension of the liquid.

3.5 RGB Analysis

3.5.1 Acid/Base Bromocresol Green Measurements

An alternative method for signal recognition is to introduce a remote digital camera to monitor the colour status of the sensor. The colour response of the sensor can then be recorded as the sensor is moved between calibration and sampling environments, through extrapolation of the RGB values associated with pixels in still images of the video footage.

The position of the sensor was controlled by the potentiostat, with a cyclic voltammetry signal being applied between ±1V to bring the sensor smoothly from one environment to the other. Because the CV technique was used the actuator's movement was slow but steady, rather than the rapid switching associated with square-wave voltammetry. This was necessary for controlled analysis of the colour change using video footage. The cycle concerned the actuator being placed between two beakers; one containing concentrated acetic acid (30% (v/v)) and the other a 0.3M ammonia solution (See Figure 3.30). The sensor was not immersed in the solution; it was instead maintained in the gas phase above the acidic/basic environments, thus activating the dye. The associated colour change that was noted across the cycle ranged from the yellow-coloured fully protonated form in the acidic environment, through a grey-blue neutral state colour in air to the fully deprotonated lazuli colour in the presence of the volatile base. One of the key advantages to using the video analysis technique is that there is no necessity for the same extent of precise control as is required to reproducibly locate the sensor between two LEDs. It is also capable of seeing many sensors in its field of view at the one time. The response that the technique is capable of demonstrating proves the principal as an alternative colorimetric technique for analysis of an actuator-based sensing system.

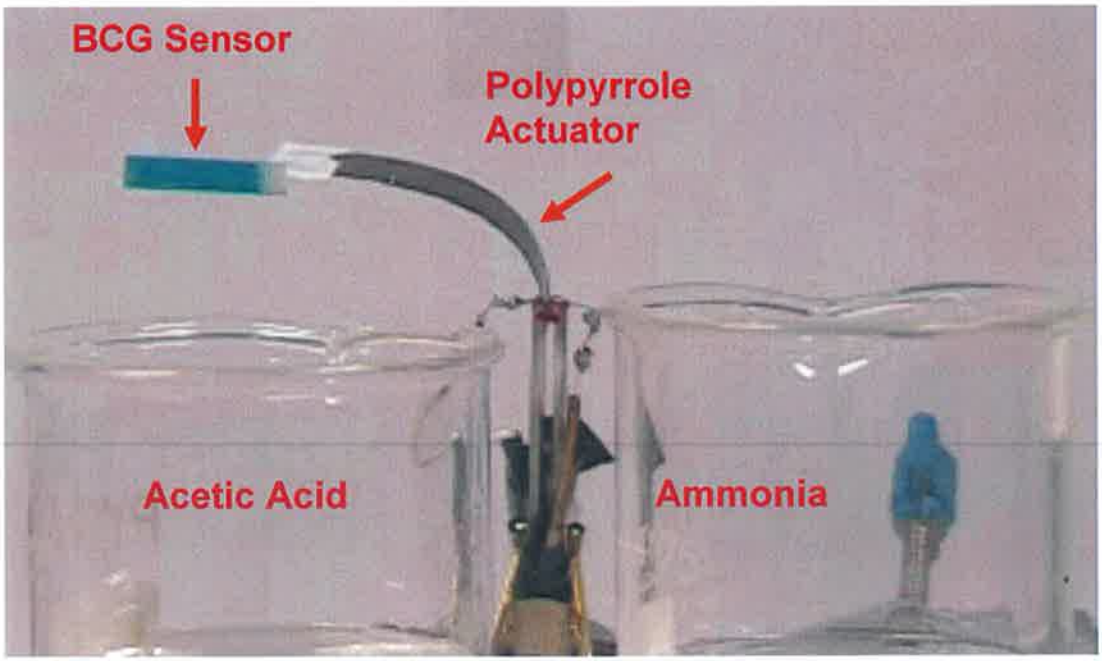

Figure 3.30: Photograph of the setup used in the initial experiments with the digital camera to monitor the sensor-actuator system.

From the video footage taken of the experiment in action over a number of cycles images were taken over a single cycle at two-second intervals. A single cycle itself lasted a period of about 40 seconds, resulting in an analysis composed of measurements in ammonia through air to acetic acid and back again, encompassing all the colour changes that occur in the dye during a cycle of the actuator. From these image files Paint Shop Pro 5 was used to isolate a 12 x 24 pixel segment from the tip of the BCG sensing substrate, which was subsequently broken into five 3 x 4 pixel segments for analysis of RGB content. The average obtained from these five readings was then represented in graphical form to show the response of the data to the colour changes in the dye. Figure 3.31 shows a summary of the technique applied to the data assimilation while Figure 3.32 shows the response generated from each of the colour components within the dye, based on each of the three isolated colour components.

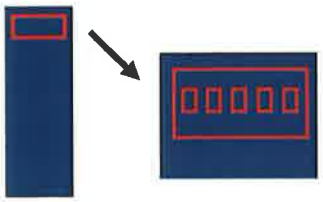

Five 3 x 4 pixel rectangular segments were taken from a 12 x 24 area segment at the tip of the sensing substrate.

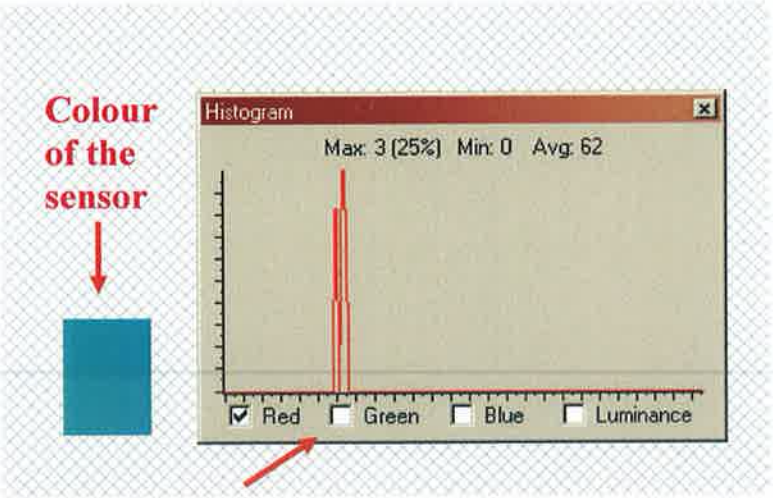

RGB analysis of sensor colour

An average RGB value was taken from the five segments using Paint Shop Pro.

	A	B	C	D	E	F	G
1	Time			0			2
2		Red	Green	Blue	Red	Green	Blue
3		60	138	145	56	128	139
4		57	137	148	61	133	143
5		57	132	148	61	135	147
6		59	131	147	62	133	151
7		69	136	149	69	135	155
8	Avg.	60.4	134.8	147.4	61.8	132.8	147
9	St.Dev.	5.0	3.1	1.5	4.7	2.9	6.3

The data is compiled under an average value for each of the three colour components separately, and is collected at 2-second intervals over a cycle-period of 40 seconds.

Therefore the Red, Green and Blue values in Figure 3.32 below derive from the mean of the five segments, with the standard deviation taken across the five terms: $\bar{x} \pm s$ (n=5)

Figure 3.31: Derivation of the average RGB values and the standard deviations.

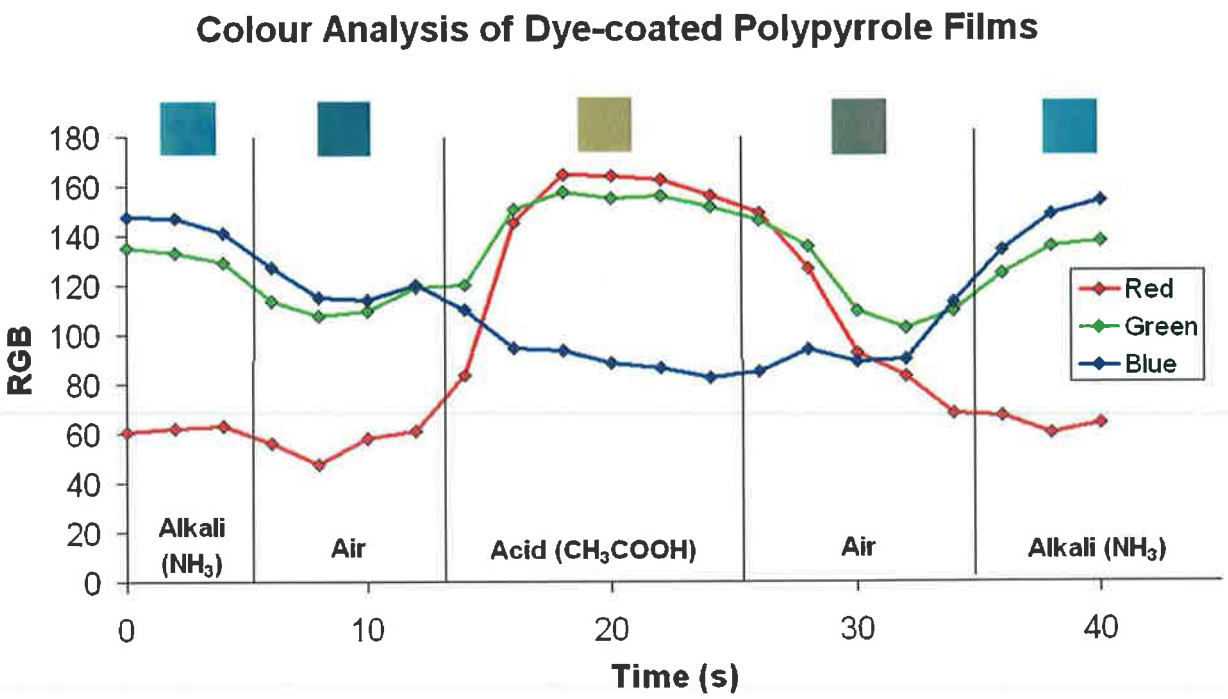

Figure 3.32: A plot of the RGB values obtained from the dye over the course of one cyclic voltammetry cycle. The coloured squares at the top of each segment represent the colour recorded at this point of the cycle.

The setup is used to demonstrate the functionality of the dye and in particularly the ability of this technique to chart the changes in colour accurately. While the two colours, and indeed the pHs represent a particularly wide range across their relative spectra it is significant nonetheless that the technique could be applied to more subtle measurements, particularly when considering the visibly small colour change at the initial basic/air interface. On the return sweep it is interesting to note that the dye retains a certain extent of its protonated yellow form, and this is reflected in the slightly differing responses shown in each of the in-air phases.

Colour	Alkali → Acid	ΔS
Red	60 → 160	+ 100
Green	130 → 160	+ 15
Blue	140 → 90	- 50

Table 3.6: Tabulation of the change in the signal that is observed when moving from one environment to another. There is an increase (ΔS) of 100 for the red data when moving the sensor from the initial alkali environment into the acid environment, for example.

The data shown above in Table 3.6 highlights the efficiency of the video technique for differentiating between the different coloured forms of the dyes. The red channel changes are clearly the most pronounced in this analysis, which can be related to the spectral changes evident in the BCG absorption plot of Figure 3.10, and will be examined further with relation to Figure 3.33. Similarly the green and blue channels will be examined in Figures 3.37 and 3.38 respectively, in reference to the spectral data. What is interesting to note is that the blue channel shows the opposite trend to that of the two other channels, due to the fact that it lies at the opposite end of the visible spectrum to red. Because the green is more mid-range of the spectrum the extent of the signal is not as strong as the red, as it lies in between the yellow and blue of the dye's protonation states.

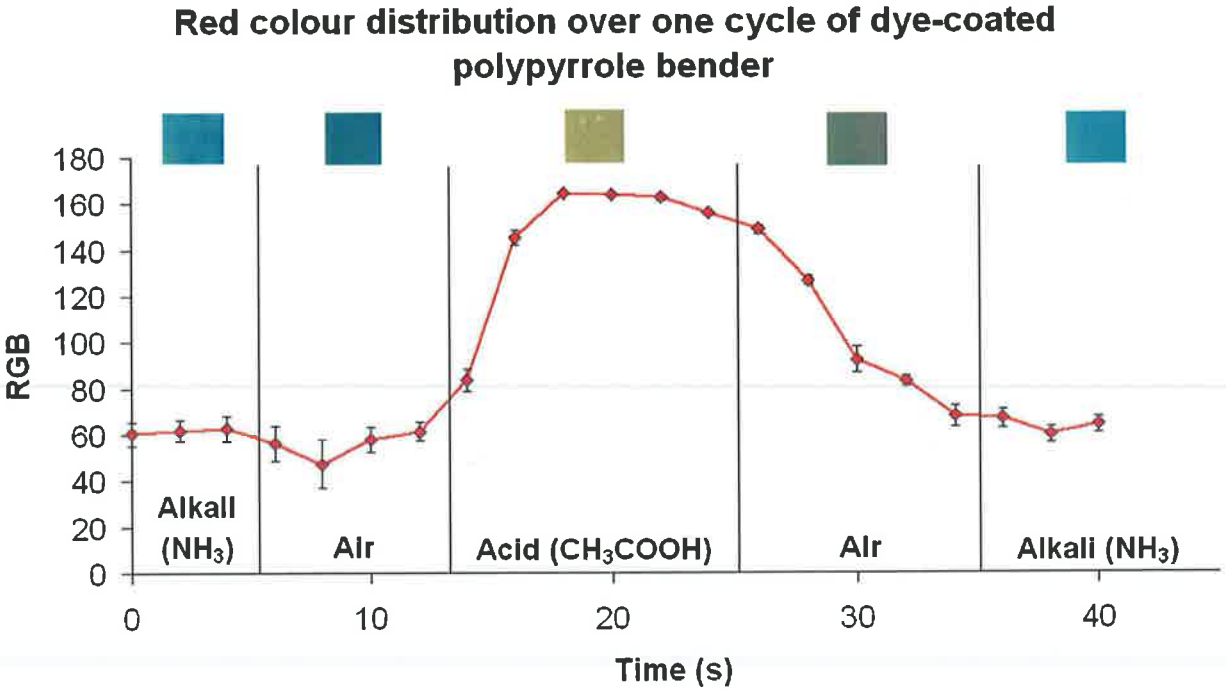

Figure 3.33: Changes in the red colour component of the RGB signal as the sensor moves through various phases.

The data shown above in Figure 3.33 shows the red data only. The initial signal is quite stable, corresponding to the actuator in stationary phase at the end point of an electrochemical cycle (run at ±1V) through to where it exits the alkali environment (NH_3). Here the sensor is exposed to ambient lab conditions where the colour changes slightly from the deprotonated basic form to a more neutral colour. Visually this corresponds to the dye changing to a less vivid blue than in the basic environment. However, in terms of the red channel of analysis there is little change between the two colours, despite the visual observation. In the acidic environment (CH_3COOH), there is a rapid change in the colour as the dye becomes yellow, with a stability in the colour change observed after 20 seconds in Figure 3.33, where the actuator has reached the vertice of the electrochemical cycle. As the cycle is switched and the actuator reverses direction, the sensor responds as it is removed from the acidic environment to ambient lab conditions. The change is more gradual moving back through to the basic environment where the signal stabilises once again.

These observations correspond well to the spectrum of BCG (Figure 3.10), as in acidic conditions there is a low absorbance of red light but large absorbance in basic

conditions. This is reflected in Figure 3.32 with the high signal of red RGB data obtained from the acidic environment and the low signal from basic conditions.

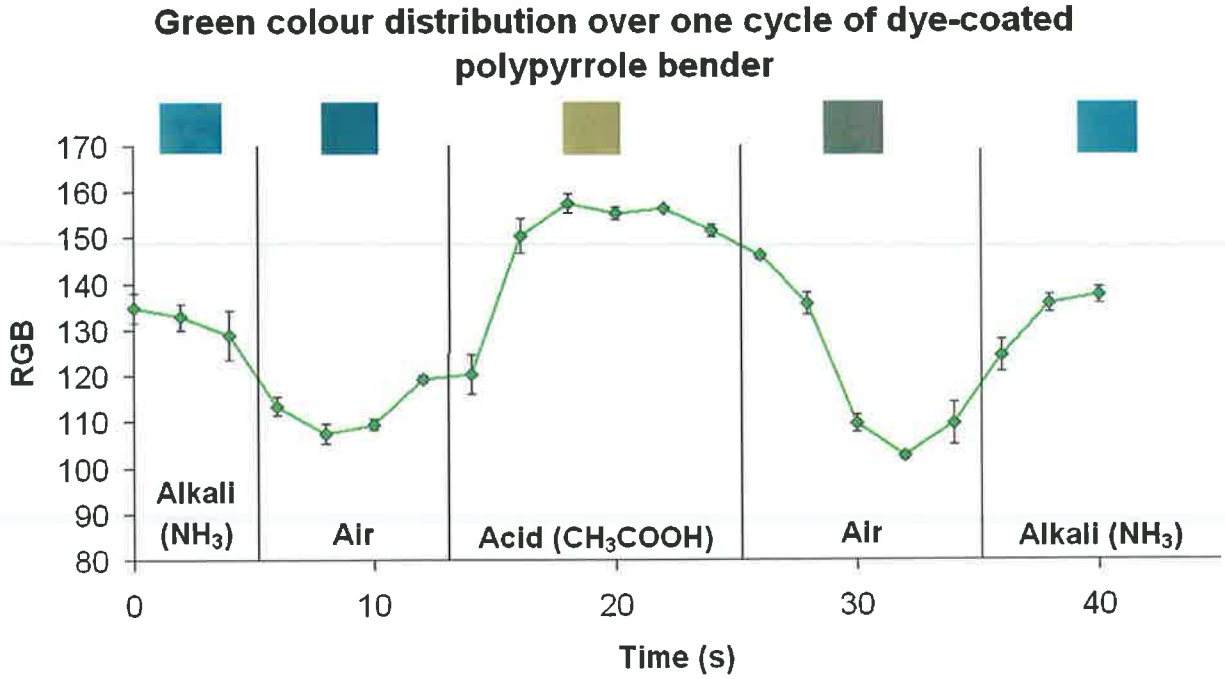

Figure 3.34: Changes in the green colour component of the RGB signal as the sensor moves through various phases.

The data for the green channel of the experiment shows that the basic and acidic forms of the dye both have a high signal. Because green lies between yellow and blue on the visible spectrum (At around 500-550nm) there is likely to be absorption in the case of either form of the dye. This can be further substantiated by Figure 3.10. However, the absorption in both cases is intermediate, lying away from the absorption maxima of the acidic and basic peaks. From the spectrum it can be seen that there is a greater extent of absorption due to the basic peak, corresponding to less of the green light being reflected back to the video camera to be measured by the computer program. This can be clearly seen in Figure 3.34 above where the signal for the alkali form is lower than that of the acidic form. In the ambient lab environment, indicated by the 'air' region of the figure above, the signal is seen to drop significantly. Visually the colours are darker, suggesting that there is more absorption of visible light across all wavelengths, resulting in the lower signal being received by the video camera as seen here.

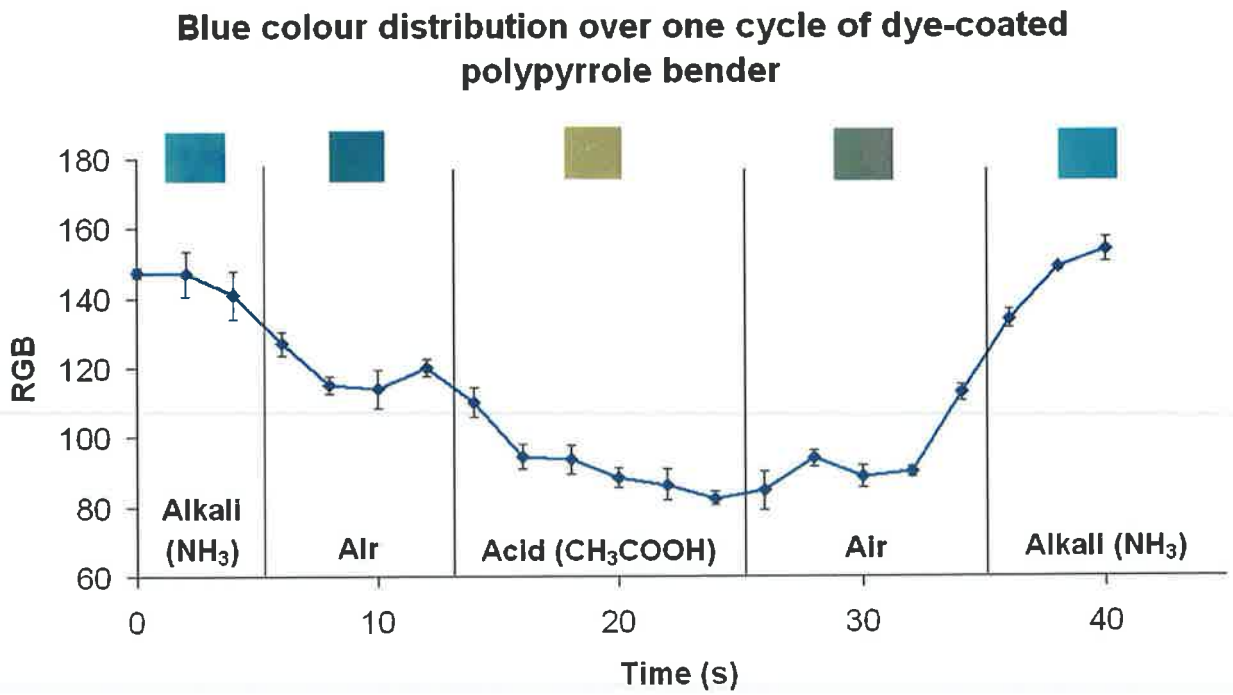

Figure 3.35: Changes in the blue colour component of the RGB signal as the sensor moves through various phases.

The blue data of Figure 3.35 shows a complete inverse effect when compared to the red data. According to the spectrum of Figure 3.10 the basic form of the dye absorbs strongly in the red region of the spectrum but not in the 450-295nm range of blue light. Because this component of the light is reflected from the dye, and hence picked up by the video camera, the signal for the dye in the alkali region of Figure 3.35 is high. Conversely, because there is a high absorbance of yellow light (570-590nm), corresponding to the acidic form of the dye, there is a concomitant low signal in the data plotted above for this region.

The significance of the data presented above is that a low cost video camera setup can potentially be used to monitor the status of many colorimetric sensors in a specific environment. The application of video monitoring technology has been applied successfully through CCTV, of which there are about 400,000 employed in London on private premises[78]. The data presented here also corroborates the use of the polypyrrole actuator for sensing purposes, again demonstrating a technique that could be employed in a self-calibrating design. The autonomous monitoring of the change in the local environment of the dye can be charted by the video camera through the medium of colour

response, while the electromechanical functionality of the polymer actuator can be used to calibrate the sensing material between measurements. In terms of the detection mechanism, one advantage of this technique over the LED-detection approach lies in less precision being involved with the sensor delivery. With the dual emitter-detector LED setup it was necessary that the sensor be delivered between the two LEDs, which were necessarily close together, requiring a great deal of actuator precision and the use of a guide. In the case of the video analysis technique, this fine precision becomes less of an issue, as the sensor is only required to be introduced to the analysis environment, with the video camera being placed at a distance capable of measurements.

3.5.2 Development of a Multisensor Array

The results achieved with the single actuator and sensor system described above led to a more advanced concept of developing a multisensor array device capable of undertaking multiple measurements at the one time. Visual analysis was ideal for this purpose as it was capable of encompassing all of the sensors simultaneously. For the LED format this method would be difficult to implement, as it would require separate dual LED emitter/detector configurations for each sensor.

The setup for this technique consisted of folded-over plastic to hold the actuators in place, to which electrical contact was provided by incorporating a series of holes through which a thin piece of platinum wire was threaded. This wire was threaded at intervals corresponding to the width of the actuators, thereby providing contact to both sides while subsequently being threaded outside of the plastic to avoid shorting of the circuit at the spaces in between. The schematic is shown in Figure 3.36 and a photograph of the device is shown in Figure 3.37. The actuators were of 2x20mm dimensions, with the sensing tips measuring in at 3x8mm, and each actuator was held firmly in position by placing a small magnet on either side of the support where the connection was made.

The receptacles for the acetic acid and ammonia environments were created by using small weighing boats, covered mostly by a glass slide but with a small gap to ensure that the volatile gas was channelled to a suitable exposure point for the sensors. The actuators were switched by the potentiostat, using the application of specific potentials for varying amounts of time. The initial applied potential waveform and current response is shown in Figure 3.38, where pulses of ±1V were followed by 10-

second periods of zero potential to allow the actuators to relax to a position where the cameras from either side could capture an image. The setup of the experiment is shown in the schematic of Figure 3.39.

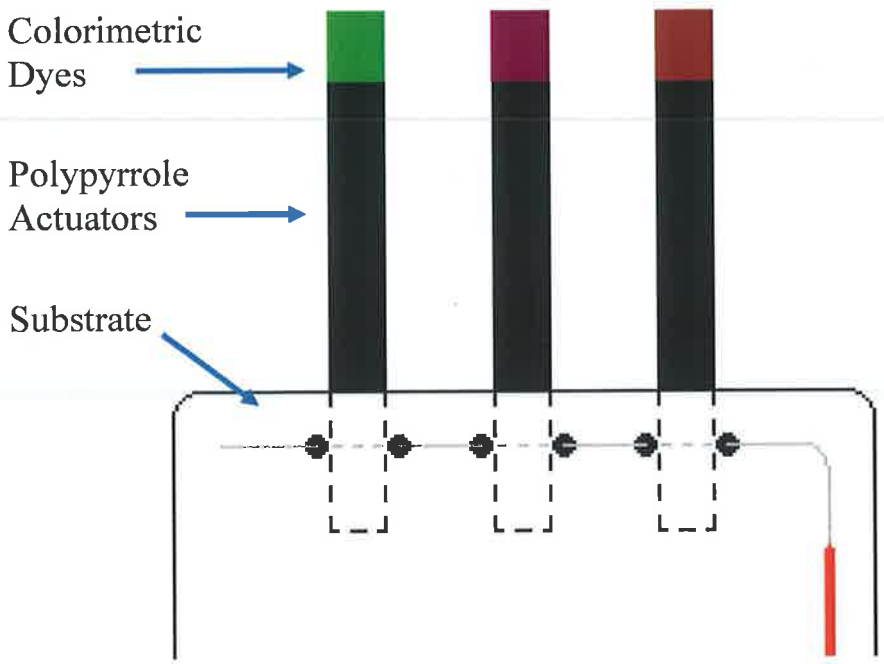

Figure 3.36: Schematic of the multisensor array setup. The substrate signifies two small sheets of polyethylene that are employed to hold the actuators in places and provide a platform to support electrical connection. A thin wire is woven through the support on both sides, connecting with each actuator (shown by the broken grey line) and threaded outside of the support in between to prevent bridging the circuit (shown by the full grey line). In this fashion connection was made to each actuator separately on a single support, and separate sensing readings could be made simultaneously using different sensors on the tips of the actuators.

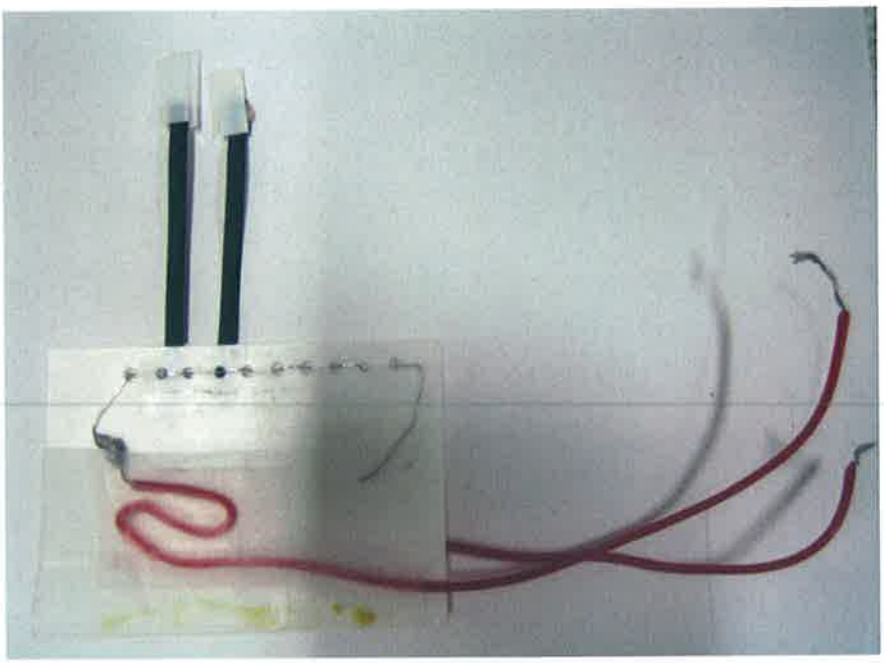

Figure 3.37: Photo schematic of the support used to house the separate actuators of the multisensor array.

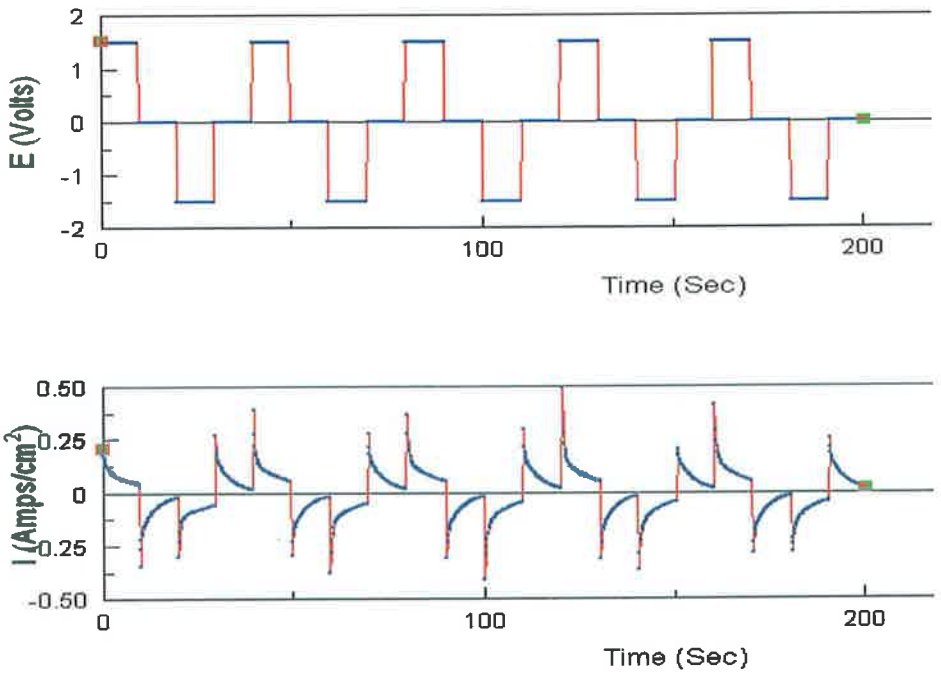

Figure 3.38: Potential waveform and current response used in the initial measurements using the multisensor array.

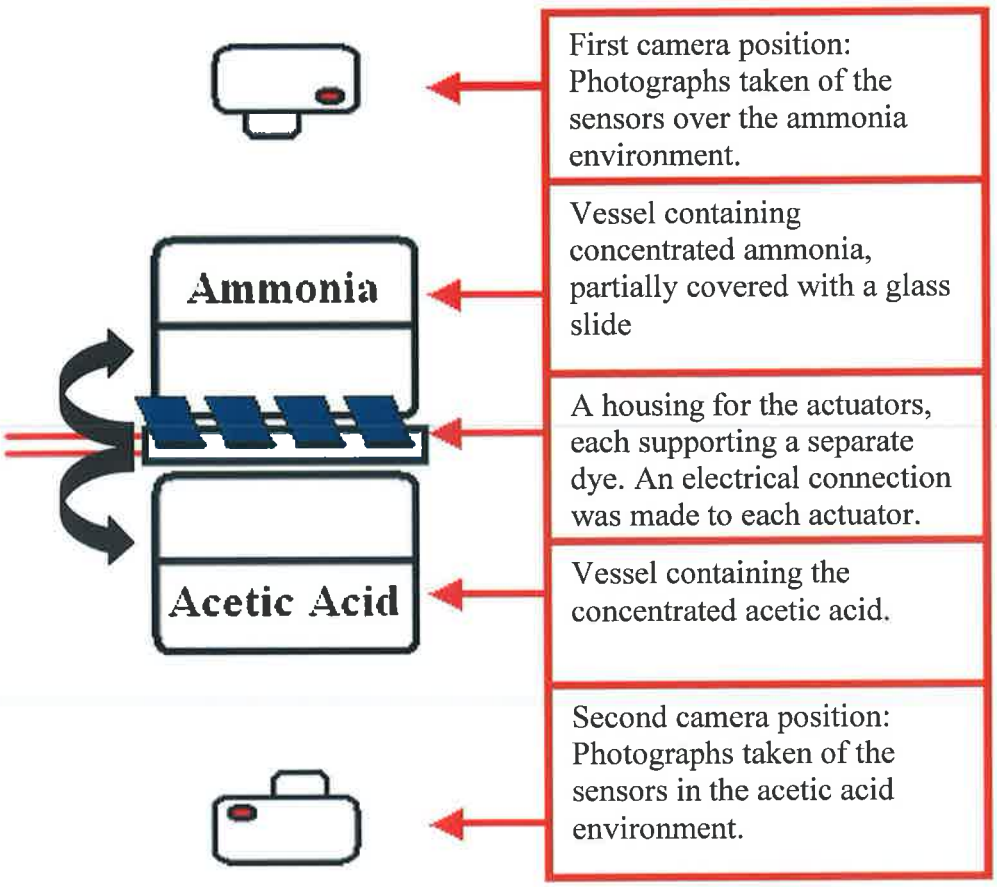

Figure 3.39: Schematic of the location of the components involved in the multisensor array. The actuators were held together between two thin sheets of plastic through which a wire had been woven to provide the connections. Electrical stimulation of the actuators at ±1V brought the sensors back and forth between the acidic and basic environments, as indicated by the two black arrows.

Information can be harvested using low power digital camera networks, such that several sensors can be simultaneously monitored using a single camera. The dyes chosen for the work exhibited differing pK_a values, though the analytes used were of strong acidity and basicity, and colour changes were generally rapid. The technique describes a simple pH sensing experiment but the concept could also be applied to more analyte-specific materials.

The setup involved the actuators all being connected to a single power source, through the use of wire woven through a plastic support substrate, as shown in Figure 3.36. The potential difference was thus maintained across the materials, with equal charge on each actuator, prompting simultaneous actuation. The movement of each of the actuators was not always symmetrical, due possibly to deviations in the homogeneity across each of the polypyrrole films. Results were obtained despite this using bromocresol green, bromocresol purple and m-cresol purple as the pH-sensitive dyes.

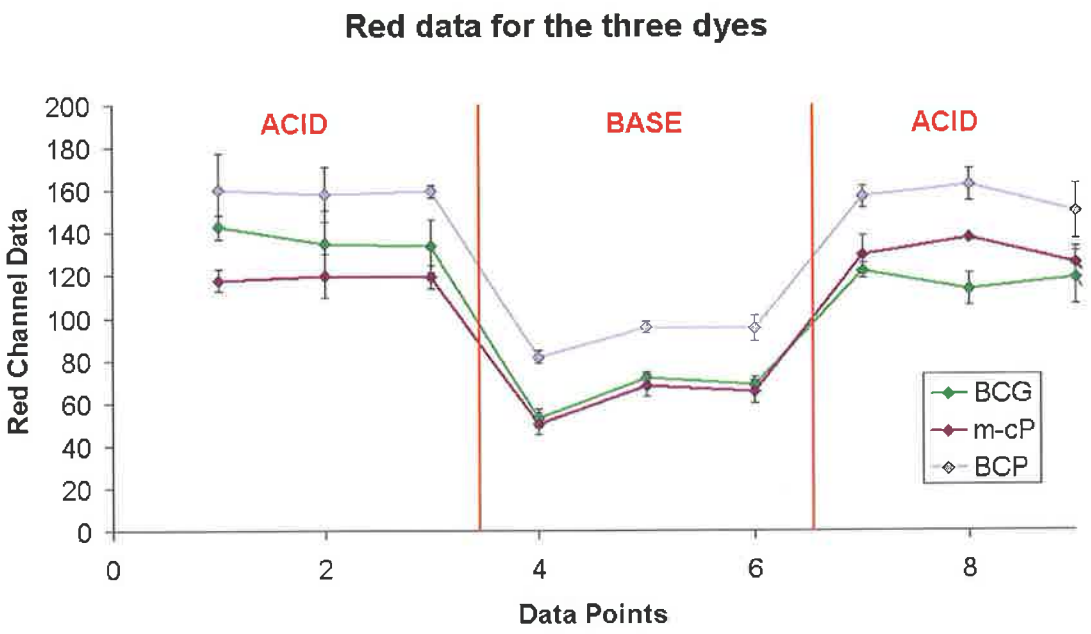

Figure 3.40: Changes in the red colour components of the dye signals as the sensor moves through various phases.

Figure 3.40 is an examination of the red colour channel for the three dyes that were used in the experiment. The plot is generated in a straightforward fashion; there are

three images taken per environment, and hence three data points per segment shown above in Figure 3.40. The first segment refers to results obtained in the acidic environment, the second in the basic environments and the final again in the acid. Each point corresponds to three separate data readings received from a single image, and thus n=3.

The data for the bromocresol green in Figure 3.40 can be compared to that from the previous experiment shown in Figure 3.33, and it is notable that the signal for the acidic form here (detector signal of 140) is not quite to the extent that it was then (detector signal of 160), although the basic form yields more or less the same values.

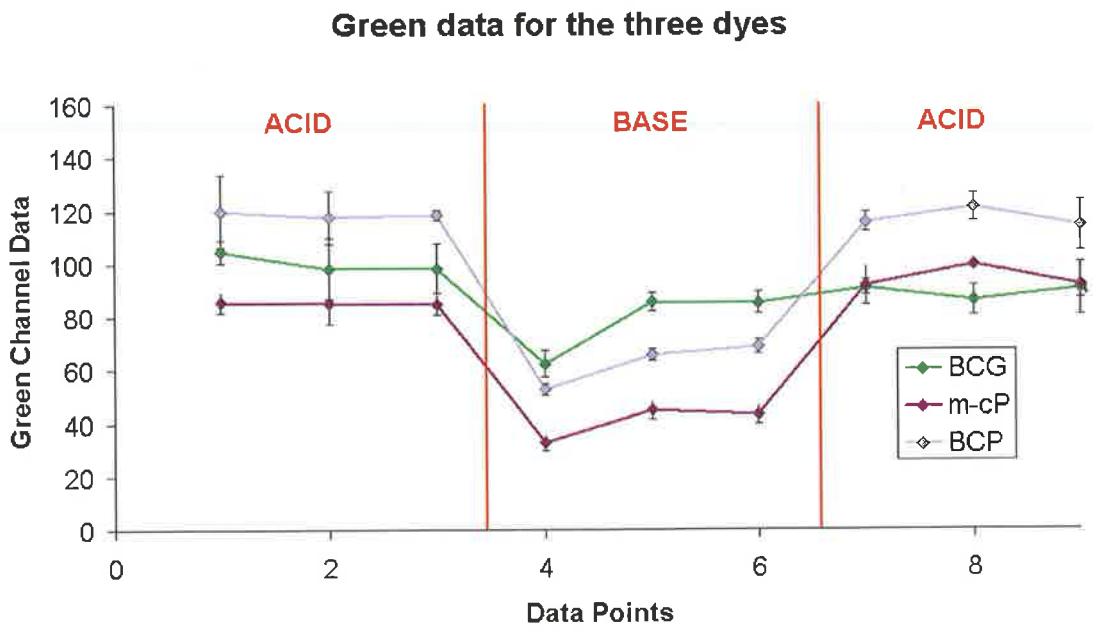

Figure 3.41: Changes in the green colour components of the dye signals as the sensor moves through various phases.

The green and blue data from Figures 3.41 & 3.42 can also be compared to their earlier equivalents in Figures 3.37 & 3.38. The interesting point on the green data in Figure 3.34 was that it had a quite high basic value but decreased in air before rising again in the acid. This explains why the green data for bromocresol green in Figure 3.41 is represented by an almost unchanging line. This is particularly noticeable when compared to the data for bromocresol purple and m-cresol purple, both of which show

distinct signal changes between acidic and basic media. When relating these observations to the visible spectrum for the acidic and basic forms of bromocresol purple (Figure 3.11) it can be seen that at the wavelength for green light (500-550nm) there is very little absorption in the acidic form, corresponding to the high signal shown in figure 3.41. There is more absorption due to the basic form, hence the dip in signal. For m-cresol purple (Figure 3.12), there is a similar relationship, through the signal in Figure 3.41 is not as strong.

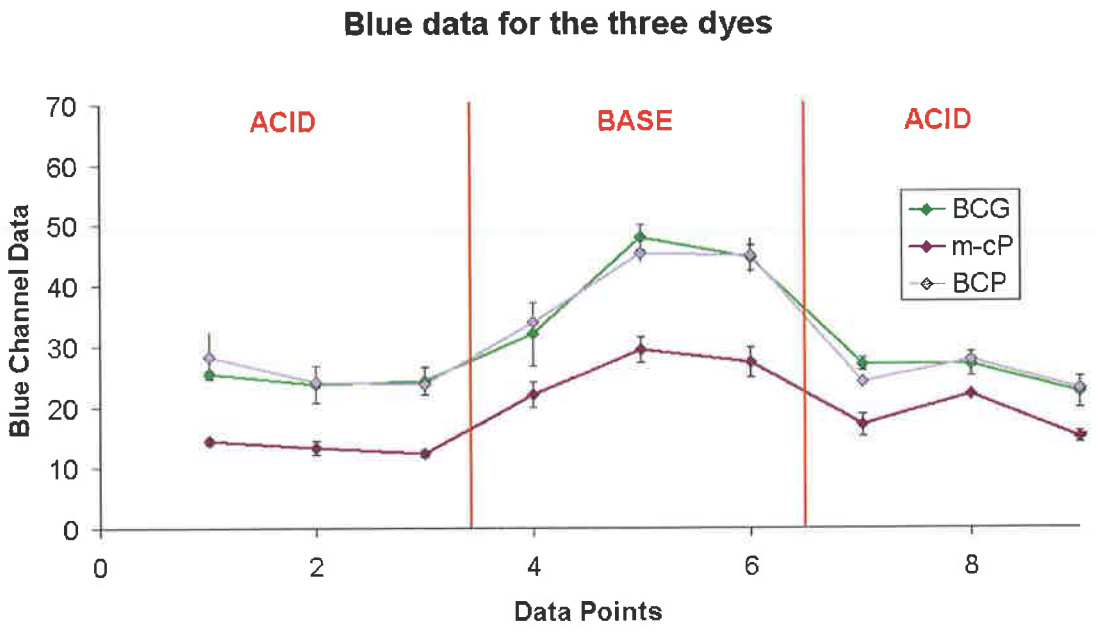

Figure 3.42: Changes in the blue colour components of the dye signals as the sensor moves through various phases.

The blue data in Figure 3.42 shows that there is a rise in the signal moving from acid into base, and this is again comparable to results generated from the single BCG sensor employed in Figure 3.35.

There is a similar signal response for each of the three dyes used. In the case of the BCG (Spectrum shown in Figure 3.10) the pattern of the obtained signals are similar to those obtained from the results using a single actuator (Shown in Section 3.5.1). The acidic environment again shows an increase in the RGB data for the red channel in Figure 3.40, due to low absorbance in the λ = 600-650nm range. The lower signal in the basic

environment is due to high absorption around the wavelength of red light (λ = 600-650nm). The data for the green channel (Figure 3.41) shows a steady signal between acidic and basic media due to similar amounts of absorption around λ = 500-550nm. The blue channel data (Figure 3.42) shows an inverse of the data obtained for the red channel, whereby greater absorbance of blue light in the acidic form yields a lower signal in the blue channel of the RGB analysis.

The BCP spectrum (Figure 3.11) shows a similar trend to the BCG data in the red and blue channels (Figures 3.40, 3.42) but there is a greater definition between the signal obtained for the green channel (Figure 3.41). This can be explained by the higher absorbance of the green light (λ = 500-550nm) in the basic form of the dye, which yields a lower signal on the green channel graph.

This pattern observed for BCP is again evident in the mCP data from Figures 3.40-3.42, and is due to similar trends in the absorbance spectrum (Figure 3.11). A summary of the data and the difference in the signals between the acidic and basic forms of the dyes can be seen in the following table.

	Acid		Base		ΔS	
	Average	St. Dev	Average	St. Dev		
Red	127.67	11.41	64.33	10.02	63.33	BCG
Green	94.83	6.82	78.00	13.86	16.83	
Blue	24.83	1.94	41.67	8.50	-16.83	
Red	157.67	4.13	90.67	7.51	67.00	BCP
Green	117.67	2.58	62.67	8.50	55.00	
Blue	25.17	2.23	41.33	6.35	-16.17	
Red	124.83	7.36	61.00	9.64	63.83	mCP
Green	89.67	5.72	40.33	6.43	49.33	
Blue	15.50	3.62	26.00	3.61	-10.50	

Table 3.7: Data for the three dyes in each of the three RGB colour channels. The ΔS column refers to the difference between the average acidic data value and the average basic data value.

4. Conclusions

The work that has been undertaken focused upon the advent of a colorimetric sensor that was capable of displaying a working capacity for self-calibration based on two separate detection mechanisms. The self-calibration potential was focused towards the use of a trilayer polypyrrole actuator, capable of moving a sensor from one environment to another using only very low power sources (±1V). The sensors applied to the analysis were based on the colorimetric response of the pH-responsive dyes bromocresol green (BCG), bromocresol purple (BCP), m-cresol purple (mCP) and bromothymol blue (BTB). The detector systems employed involved a simple, low-cost emitter/detector LED setup and a continuous video analysis setup.

The LED setup was first adapted for the analysis of the response of BCG over time, using acetic acid as the analyte and ammonia as the calibrant. The dye was coated to a polyethylene substrate that was then applied to the end of a polypyrrole actuator, which moved the sensor from one environment to another. The detector system was set up inside the acetic acid environment, and the response was measured as the sensing tip was brought in between the emitter and detector LEDs. Results showed the response when moving from a basic to an acidic environment, and how the rate of change varied over time. Despite a gradual tail off in the sensitivity, a clear signal was still evident after 2 hours, demonstrating the potential of the device for self-calibrated sensing.

The LED systems was also employed to analyse the change in a BTB-coated substrate using solution-based sensing. The BTB was found to demonstrate very little by way of the dye leaching into solution, only having being left submerged for days was this seen to occur. A range of pH standards were prepared and the sensor was left to equilibrate for 10 minutes before being introduced to the LED system. A manual method (where the sensor was placed by hand into the detector system) and an actuator-based sensor delivery method were applied and the results were drawn up by way of a sigmoid plot. A first derivative curve was drawn up to show the pK_a of the dye, where the protonated and deprotonated forms of the BTB were in equilibrium. The results showed slight deviations from the literature value but again proved the actuator-based sensor was capable of delivering a sensor from one environment to a detector. This could again be applied to a self-calibrating system where the solution would act as a calibrant and the analyte would be based around the detector.

The video analysis was firstly based around a single actuator-based BCG sensor. A video was taken across a cycle of the system, from ammonia to acetic acid and back to ammonia again. Paint Shop Pro software was used to analyse the RGB data of the sensor at 2-second intervals across the cycle, and the data was divided up into its red, green and blue components for analysis. Comparison of the data acquired to the spectrum of the dye revealed agreement in the response of the system, and suggested that a detector system based on remote video analysis could be applied to a calibrant system developed from this concept. The idea was developed to include three separate dyes on a similar manifold, with Paint Shop Pro software again used to extrapolate the data based on BCG, BCP and mCP dyes. The initial results were again promising in that there was again agreement with the spectral data, although modification of the system setup is necessary. With this technique, a single camera could be employed to monitor multiple sensors, whose status can be regularly checked by moving between the sampling and the reference environment. This technique can furthermore be expanded through the networking of multiple cameras, similar to CCD networks in London, which are estimated to consist of over 80,000 alone.

The experiments have shown positive results in the application of a polypyrrole-based actuator system for self-calibration in chemical sensing, and have displayed two separate detection methods capable of harvesting data from the setup.

5. Acknowledgements

I would like to thank Professor Dermot Diamond for allowing me the opportunity to study in the Adaptive Sensors Group (ASG) in DCU, and for the support and guidance he has given me throughout my time here. Rod, Kim and Sonia I would like to thank for their help during the project, and for many chats over coffee regarding the direction of the project, and for solving many issues I had. I would like to thank everybody I have had the pleasure of working with in the ASG as they have in a big way helped to make it possible that I complete the work to this point.

In the Intelligent Polymer Research Institute of the University of Wollongong I would like to thank Professor Gordon Wallace for allowing me the opportunity to study in the institute for a 2-month stint, and for the continuing collaboration on the project. To Richard I owe more than I could ever repay for his help both with the experimental side of the project and for the lengthy talks on the nature of research and beyond.

I would also like to thank everyone else who has been a part of my life during this time; everyone has been supportive in their own way!

6. Publication Details

Papers:

Title: Self-Maintained Colorimetric Acid/Base Sensor Using Polypyrrole Actuator

Authors: Ciarán Smyth, King Tong Lau, Roderick L. Shepherd, Dermot Diamond, Yanzhe Wu, Geoffrey M. Spinks, Gordon G. Wallace

Journal: Sensors & Actuators B

Date: September 10, 2007

Poster Presentations:

Title: Electroactive polymers for fluid movement

Authors: Ciarán Smyth, King Tong Lau, Dermot Diamond, Jenny Causley, Yanzhe Wu, Gordon Wallace

Conference: The Wollongong Workshop on Nanostructured Electromaterials, University of Wollongong

Date: February 3rd – 4th, 2005

Title: Conducting Polymers for use in microfluidics and chemical sensing

Authors: Ciarán Smyth, King Tong Lau, Dermot Diamond, Jenny Causley, Yanzhe Wu, Gordon Wallace

Conference: Irish Research Council for Science, Engineering and Technology National Symposium

Date: November 3rd, 2005

Title:	Autonomous Sensing using Trilayer Polypyrrole Actuators
Authors:	Ciarán Smyth, Yanzhe Wu, Sonia Ramirez-Garcia, Rod Shepherd, King Tong Lau, Gordon Wallace, Dermot Diamond
Conference:	Irish Universities Chemistry Research Colloquium
Date:	June 14th - 16th, 2006

Title:	Autonomous Sensing using Trilayer Polypyrrole Actuators
Authors:	Ciarán Smyth, Yanzhe Wu, Sonia Ramirez-Garcia, Rod Shepherd, King Tong Lau, Gordon Wallace, Dermot Diamond
Conference:	International Conference on Synthetic Metals
Date:	July 2 - 7, 2006

7. References

[1] Cadogan, A. M.; Diamond, D.; Smyth, M. R.; Deasy, M.; Mckervey, M. A.; Harris, S. J. *Analyst* **1989**, *114*, 1551-1554

[2] Cadogan, F.; Kane, P.; McKervey, M. A.; Diamond, D. *Analytical Chemistry* **1999**, *71*, 5544-5550

[3] McCarrick, M.; Wu, B.; Harris, S. J.; Diamond, D.; Barrett, G.; Mckervey, M. A. *Journal of the Chemical Society-Perkin Transactions 2* **1993**, 1963-1968

[4] Schazmann, B.; McMahon, G.; Nolan, K.; Diamond, D. *Supramolecular Chemistry* **2005**, *17*, 393-399

[5] Brady, S.; Diamond, D.; Lau, K. T. *Sensors and Actuators a-Physical* **2005**, *119*, 398-404

[6] Dunne, L.; Brady, S.; Smyth, B.; Diamond, D. *Journal of Neuroengineering Rehabilitation* **2005**, *2*, 4

[7] Hisamoto, H.; Tohma, H.; Yamada, T.; Yamauchi, K.; Siswanta, D.; Yoshioka, N.; Suzuki, K. *Analytica Chimica Acta* **1998**, *373*, 271-289

[8] Peterson, J. I.; Vurek, G. G. *Science* **1984**, *224*, 123-127

[9] Seitz, W. R. *Analytical Chemistry* **1984**, *56*, A16-&

[10] Bissell, R. A.; Desilva, A. P. *Journal of the Chemical Society-Chemical Communications* **1991**, 1148-1150

[11] McEvoy, A. K.; McDonagh, C. M.; MacCraith, B. D. *Analyst* **1996**, *121*, 785-788

[12] McDonagh, C.; MacCraith, B. D.; McEvoy, A. K. *Analytical Chemistry* **1998**, *70*, 45-50

[13] McDonagh, C.; Kolle, C.; McEvoy, A. K.; Dowling, D. L.; Cafolla, A. A.; Cullen, S. J.; MacCraith, B. D. *Sensors and Actuators B-Chemical* **2001**, *74*, 124-130

[14] Malins, C.; MacCraith, B. D. *Analyst* **1998**, *123*, 2373-2376

[15] Malins, C.; Niggemann, M.; MacCraith, B. D. *Measurement Science & Technology* **2000**, *11*, 1105-1110

[16] von Bultzingslowen, C.; McEvoy, A. K.; McDonagh, C.; MacCraith, B. D.; Klimant, I.; Krause, C.; Wolfbeis, O. S. *Analyst* **2002**, *127*, 1478-1483

[17] Lau, K. T.; Baldwin, S.; Shepherd, R. L.; Dietz, P. H.; Yerzunis, W. S.; Diamond, D. *Talanta* **2004**, *63*, 167-173

[18] Lau, K. T.; Baldwin, S.; O'Toole, M.; Shepherd, R.; Yerazunis, W. J.; Izuo, S.; Ueyama, S.; Diamond, D. *Analytica Chimica Acta* **2006**, *557*, 111-116

[19] Allain, L. R.; Canada, T. A.; Xue, Z. L. *Analytical Chemistry* **2001**, *73*, 4592-4598

[20] Matias, F. A. A.; Vila, M. M. D. C.; Tubino, M. *Sensors and Actuators B-Chemical* **2003**, *88*, 60-66

[21] Benson, R. L.; Worsfold, P. J. *Science of the Total Environment* **1993**, *135*, 17-25

[22] Tian, K.; Dasgupta, P. K. *Analytical Chemistry* **1999**, *71*, 2053-2058

[23] Oshima, M.; Wei, Y. L.; Yamamoto, M.; Tanaka, H.; Takayanagi, T.; Motomizu, S. *Analytical Sciences* **2001**, *17*, 1285-1290

[24] Diamond, D. *Analytical Chemistry* **2004**, *76*, 278a-286a

[25] Edmonds, T. E., Ed.; Blackie and Son Ltd: New York, 1988

[26] Mainwaring, A.; Polastre, J.; Szewczyk, R.; Culler, D.; Anderson, J. In *Proceedings of the first ACM international workshop on wireless sensor networks and applications* Atlanta, Georgia, USA, September 28, **2002**, p 88-97

[27] http://www.greatduckisland.net

[28] Arora, A.; Ramnath, R.; Sinha, P.; Ertin, E.; Bapat, S.; Naik, V.; Kulathumani, V.; Zhang, H. W.; Sridharan, M.; Kumar, S.; Cao, H.; Seddon, N.; Anderson, C.; Herman, T.; Zhang, C.; Trivedi, N.; Gouda, M.; Choi, Y. R.; Nesterenko, M.; Shah, R.; Kulkarni, S.; Aramugam, M.; Wang, L. M.; Culler, D.; Dutta, P.; Sharp, C.; Tolle, G.; Grimmer, M.; Ferriera, B.; Parker, K. *Distributed Computing in Sensor Systems, Proceedings* **2005**, *3560*, 393-394

[29] Shirakawa, H.; Louis, E. J.; Macdiarmid, A. G.; Chiang, C. K.; Heeger, A. J. *Journal of the Chemical Society-Chemical Communications* **1977**, 578-580

[30] Chiang, C. K.; Fincher, C. R.; Park, Y. W.; Heeger, A. J.; Shirakawa, H.; Louis, E. J.; Gau, S. C.; Macdiarmid, A. G. *Physical Review Letters* **1977**, *39*, 10981101

[31] Chiang, C. K.; Druy, M. A.; Gau, S. C.; Heeger, A. J.; Louis, E. J.; Macdiarmid, A. G.; Park, Y. W.; Shirakawa, H. *Journal of the American Chemical Society* **1978**, *100*, 1013-1015

[32] Reynolds, J. R. *Chemtech* **1988**, *18*, 440-447

[33] Diaz, A. F.; Kanazawa, K. K.; Gardini, G. P. *J. Chem. Soc., Chem. Comm.* **1979**, 635-636

[34] Street, G. B.; Lindsey, S. E.; Nazzal, A. I.; Wynne, K. J. *Molecular Crystals and Liquid Crystals* **1985**, *118*, 137-148

[35] Street, G. B.; Clarke, T. C.; Geiss, R. H.; Lee, V. Y.; Nazaal, A. I.; Pfluger, P.; Scott, J. C. *J. Physique.* **1983**, *C3*, 599

[36] Nazaal, A. I.; Street, G. B. *J. Electroanal. Chem.* **1983**, *27*, 342

[37] Andrieux, C. P.; Audebert, P.; Hapiot, P.; Saveant, J. M. *Journal of Physical Chemistry* **1991**, *95*, 10158-10164

[38] John, R.; Wallace, G. G. *Polymer International* **1992**, *27*, 255-260

[39] Ogasawara, M.; Funahashi, K.; Iwata, K. *Molecular Crystals and Liquid Crystals* **1985**, *118*, 159-162

[40] Baughman, R. H. *Synthetic Metals* **1996**, *78*, 339-353

[41] Wu, Y. Ph.D. Thesis, University of Wollongong, 2006

[42] Madden, J. D.; Cush, R. A.; Kanigan, T. S.; Hunter, I. W. *Synthetic Metals* **2000**, *113*, 185-192

[43] Wallace, G. G.; Spinks, G. M.; Kane-Maguire, L. A. P.; Teasdale, P. R. *Conductive Electroactive Polymers - Intelligent Materials Systems*; CRC Press, 2003

[44] Wu, J. Y., L; Xu, H.; Tang, W.C.; Zeng, F-G. In *Transducers '05: The 13th International Conference on Solid-State Sensors, Actuators and Microsystems* Seoul, Korea, June 5-9, 2005, p 1636-1639

[45] Baughman, R. H.; Shacklette, L. W.; Elsenbaumer, R. L.; Plichta, E. J.; Becht, C. In *Conjugated Polymer Materials: Opportunities in Electronics, Optoelectronics and Molecular Electronics* Kluwer, Dordrecht, 1990, p 559-582

[46] Andrieux, C. P.; Audebert, P.; Hapiot, P.; Nechtschein, M.; Odin, C. *Journal of Electroanalytical Chemistry* **1991**, *305*, 153-162

[47] Kobayashi, T.; Yoneyama, H.; Tamura, H. *Journal of Electroanalytical Chemistry* **1984**, *161*, 419-423

[48] Foot, P. J. S.; Simon, R. *Journal of Physics D-Applied Physics* **1989**, *22*, 1598-1603

[49] Pei, Q. B.; Inganas, O. *Advanced Materials* **1992**, *4*, 277-278

[50] Pei, Q. B.; Inganas, O. *Journal of Physical Chemistry* **1992**, *96*, 10507-10514

[51] Smela, E.; Inganas, O.; Pei, Q. B.; Lundstrom, I. *Advanced Materials* **1993**, *5*, 630-632

[52] Smela, E.; Inganas, O.; Lundstrom, I. *Science* **1995**, *268*, 1735-1738

[53] Spinks, G. M.; Liu, L.; Wallace, G. G.; Zhou, D. Z. *Advanced Functional Materials* **2002**, *12*, 437-440
[54] Madden, J. D.; Cush, R. A.; Kanigan, T. S.; Brenan, C. J.; Hunter, I. W. *Synthetic Metals* **1999**, *105*, 61-64
[55] Lu, W.; Fadeev, A. G.; Qi, B. H.; Smela, E.; Mattes, B. R.; Ding, J.; Spinks, G. M.; Mazurkiewicz, J.; Zhou, D. Z.; Wallace, G. G.; MacFarlane, D. R.; Forsyth, S. A.; Forsyth, M. *Science* **2002**, *297*, 983-987
[56] Andrews, M. K.; Jansen, M. L.; Spinks, G. M.; Zhou, D. Z.; Wallace, G. G. *Sensors and Actuators a-Physical* **2004**, *114*, 65-72
[57] Arai, H.; Muller, S.; Haas, O. *Journal of the Electrochemical Society* **2000**, *147*, 3584-3591
[58] De Rossi, D.; DellaSanta, A.; Mazzoldi, A. *Mater. Sci. Eng. C.* **1999**, *7*, 31
[59] Wallace, G. G.; Smyth, M.; Zhao, H. *Trac-Trends in Analytical Chemistry* **1999**, *18*, 245-251
[60] Reisberg, S.; Piro, B.; Noel, V.; Pham, M. C. *Bioelectrochemistry* **2006**, *69*, 172-179
[61] Barisci, J. N.; Wallace, G. G.; Andrews, M. K.; Partridge, A. C.; Harris, P. D. *Sensors and Actuators B-Chemical* **2002**, *84*, 252-257
[62] Kress-Rogers, E. E. *Handbook of Biosensors and Electronic Noses, Medicine, Food and the Environment*; CRC Press, Boca Raton, 1996
[63] Nguyen, T. A.; Barisci, J. N.; Partridge, A.; Wallace, G. G. *Synthetic Metals* **2003**, *137*, 1445-1446
[64] Ngamna, O.; Morrin, A.; Moulton, S. E.; Killard, A. J.; Smyth, M. R.; Wallace, G. G. *Synthetic Metals* **2005**, *153*, 185-188
[65] Pacquit, A.; Lau, K. T.; McLaughlin, H.; Frisby, J.; Quilty, B.; Diamond, D. *Talanta* **2006**, *69*, 515-520
[66] O'Toole, M.; Lau, K. T.; Diamond, D. *Talanta* **2005**, *66*, 1340-1344
[67] Badugu, R.; Lakowicz, J. R.; Geddes, C. D. *Talanta* **2005**, *66*, 569-574
[68] Nalwa, H. S. *Handbook of Organic Conductive Molecules and Polymers*, 1997
[69] Wu, Y.; Alici, G.; Spinks, G. M.; Wallace, G. G. *Synthetic Metals* **2006**, *156*, 1017-1022
[70] Skotheim, T.A.; Reynolds, J.R. Chapter 8, *Conducting Polymers: Theory, Synthesis, Properties, and Characteristics;* CRC Press, 2007
[71] Olmsted, J.; Williams, G. M. *Chemistry: The Molecular Science*; Mosby, 1994
[72] http://antoine.frostburg.edu/chem/senese/101/acidbase/indicators.shtml
[73] http://www.sigmaaldrich.com/catalog/search/ProductDetail/SIAL/114367
[74] http://www.ph-meter.info/pH-measurements-indicators
[75] Hurt, J. D.; Tu, C. K.; Laipis, P. J.; Silverman, D. N. *Journal of Biological Chemistry* **1997**, *272*, 13512-13518
[76] http://www.intute.ac.uk/sciences/reference/chemdata/12.html
[77] Diamond, D.; Hanratty, V. C. A. *Spreadsheet Applications in Chemistry using Microsoft Excel*; John Wiley & Sons, Inc., 1997
[78] http://en.wikipedia.org/wiki/Closed-circuit_television